



D5.8 SAFETY IMPACT ASSESSMENT-UPDATED REPORT

Primary Author(s)	Jordanka Kovaceva, Carol Flannagan Chalmers University of Technology Harald Kolk, Peter Wimmer Virtual Vehicle Lars Schories, Ellankavi Ramasamy ZF Friedrichshafen AG Julian Becker Institut für Kraftfahrzeuge (ika) Christian Loeffler Robert Bosch GmbH Jorge Lorente Mallada Toyota Motor Europe Daniel Weihmayr Technische Hochschule Ingolstadt Jacint Castells Applus IDIADA
Related Work Package	WP5
Version/Status	1.0 Final
Issue date	31/01/2023
Deliverable type	R
Dissemination Level	PU
Project Acronym	SAFE-UP
Project Title	proactive SAFETy systems and tools for a constantly UPgrading road environment
Project Website	www.safe-up.eu
Project Coordinator	Núria Parera Applus IDIADA
Grant Agreement No.	861570



This project has received funding from the European Union's Horizon 2020 research and innovation programme under Grant Agreement 861570.

Co-Authors

Name	Organisation
Johan Davidsson	Chalmers University of Technology

Document Distribution

Version	Date	Distributed to
0.8	2023-01-26	Coordination Team
1.0	2023-01-31	Submission in the EC System
		Approved by the EC



Copyright statement

The work described in this document has been conducted within the SAFE-UP project. This document reflects only the views of the SAFE-UP Consortium. The European Union is not responsible for any use that may be made of the information it contains.

This document and its content are the property of the SAFE-UP Consortium. All rights relevant to this document are determined by the applicable laws. Access to this document does not grant any right or license on the document or its contents. This document or its contents are not to be used or treated in any manner inconsistent with the rights or interests of the SAFE-UP Consortium or the Partners detriment and are not to be disclosed externally without prior written consent from the SAFE-UP Partners.

Each SAFE-UP Partner may use this document in conformity with the SAFE-UP Consortium Grant Agreement provisions.



Executive summary

The aim of the SAFE-UP project is to improve traffic safety by developing tools and innovative methods that proactively address the safety challenges of future mobility systems. This deliverable, which is the final report of the work performed in SAFE-UP task T5.3, which is part of WP5: Safety assessment methodologies, specifies methods and approaches that will be used for the assessment of the safety impact of the SAFE-UP safety technologies implemented in four demonstrators. The aim with the demonstrators is not the delivery of a ready-to-use product but rather to understand the safety potential and the limitations of the safety technologies. Deliverable 5.2 (Bálint, Schindler, et al., 2021) described the work in progress regarding the methodology while the final methodology for safety impact assessment is reported in this Deliverable D5.8.

A general framework for assessing the safety benefit of the SAFE-UP safety technologies was proposed in D5.1, built on knowledge from research publications and experience from previous projects and adapted to the specific needs of SAFE-UP. There are two essential elements in the framework. The first one is detailed pre-crash and in-crash simulations according to the principles of the Prospective Effectiveness Assessment for Road Safety (P.E.A.R.S.) initiative. The second one is combining the results of these simulations and results from physical testing in a Bayesian statistical approach developed in the EU project PROSPECT. Task 5.3 follows the structure of the framework described in D5.1 and specifies how to apply this structure to the four demonstrators.

To improve the occupant protection in case of a collision and reduce the increased risk of injury for occupants in new seating positions, e.g., reclined seatback, WP4 in the SAFE-UP project is investigating an adaptive restraint system. These restraint systems are implemented in SAFE-UP Demonstrator 1 (abbreviated as **Demo 1**). The occupant protection is evaluated virtually using both female and male Human Body Models (HBMs) in new seating positions with state-of-the-art (SOTA) and added-feature (AF) restraint systems.

Additionally, a main goal of SAFE-UP is to address the protection of Vulnerable Road Users (VRUs), primarily pedestrians and bicyclists, also targeting weather conditions that could adversely affect sensor performance (e.g., rain). Improved sensors implemented in a prototype vehicle are used in the second demonstrator in SAFE-UP (**Demo 2**). This vehicle undergoes physical testing in various weather conditions, including adverse weather conditions (e.g., precipitation of different intensity); the test results support the development of a filter representing reduced sensor performance in rain and fog which in turn is included in pre-crash simulations. These simulations enable a quantification of the reduction of crashes and (serious) injuries resulting from the ability of an Autonomous Emergency Braking (AEB) system for VRU protection to address scenarios with adverse weather conditions.

The third SAFE-UP demonstrator (**Demo 3**) includes an Autonomous Emergency Braking and Steering system (AEB+S) with full functionality for all weather conditions. The scenarios to be addressed by Demo 3 are selected by considering the theoretical possibility of avoiding



crashes by braking and steering (under given boundary conditions for these actions). The most relevant scenarios for adverse weather conditions are covered first, and the range of addressed scenarios is extended further. Representations of the safety systems for VRU protection are integrated in a co-simulation platform (i.e., different simulation tools coupled in an overall simulation) which will be used to obtain results for safety benefit assessment. The results are complemented by physical testing of the Demo 3 vehicle and further simulations addressing aspects and parameter combinations that are not feasible to cover by physical testing.

The fourth SAFE-UP demonstrator (**Demo 4**) focuses on understanding the safety benefit potential of Cooperative Intelligent Transport Systems (C-ITS). All the possible communication interactions, such as timely warnings to both VRU and driver as well as actuation of safety systems like AEB for VRU protection are considered. However, the primary focus is on timely warnings which could avoid emergency situations. The selection of scenarios for Demo 4 was based on the crash data analysis presented in D2.6 (Bálint, Labenski, et al., 2021) and considering the state-of-the-art safety systems for VRU protection and the added value of C-ITS in various scenarios based on expert assessment. Physical testing of the Demo 4 vehicle will address the identified scenarios. A virtual performance assessment will be done for the benefit of V2X as an additional “sensor node” for a vehicle system.

Finally, elements of the assessment are highlighted that are not specific to a single demonstrator, such as the combination of test results and simulation results, as well as data weighting method to extrapolate results from locally collected data to an EU level. A sensitivity analysis exploring the sensitivity of results to the specifications in the weighting method such as the variable selection for hypercube weighting is illustrated. The statistical approach from the PROSPECT project is applied in that test results and simulation results are combined in a Bayesian statistical approach, and further details of this approach are described in this report.



Table of contents

1. Introduction.....	14
1.1 <i>Literature review on injury risk functions.....</i>	15
1.1.1 Injury risk functions to assess individual body parts	15
1.1.2 Selection of injury risk functions: occupant injury assessment	18
1.1.3 Injury risk functions based on crash parameters.....	18
1.1.4 Selection of injury risk functions: frontal crashes with VRUs	19
1.2 <i>Baseline definition method.....</i>	21
1.2.1 Baseline definition, Approach B.....	22
1.2.2 Baseline definition, Approach C2.....	26
1.3 <i>Technical aspects of the implementation of investigated use-cases</i>	30
1.3.1 Setup of the use-cases P/B-CLwSO, P/B-CRwSO, with and without sight obstruction	30
1.3.2 Setup of the use-cases TurnL-SD	32
2. Demo 1.....	34
2.1 <i>Workflow – Selection of crashes.....</i>	34
2.2 <i>Simulations.....</i>	35
2.3 <i>Models for injury risk probability.....</i>	38
2.4 <i>Estimation of the safety benefit.....</i>	41
2.5 <i>Market penetration</i>	44
3. Demo 2.....	45
3.1 <i>Simulations.....</i>	45
3.1.1 Baseline.....	46
3.1.2 Simulation models.....	46
4. Demo 3.....	50
4.1 <i>Simulations.....</i>	50
4.1.1 Baseline.....	50
4.1.2 Simulation models.....	51
4.2 <i>Physical testing.....</i>	56
5. Demo 4.....	58



5.1	<i>Simulations</i>	59
5.1.1	Baseline for simulations by IDIADA.....	59
5.1.2	Baseline for simulations by ZF.....	60
5.1.3	Simulation models.....	61
5.2	<i>Physical testing</i>	64
5.2.1	Real VRUs (cyclists) using an enhanced VRU V2X device and a virtual vehicle.....	64
5.2.2	Dummy VRU platforms and real vehicle.....	65
6.	Common aspects	66
6.1	<i>Bayesian modelling</i>	66
6.1.1	Modelling the probability of crash avoidance	67
6.1.2	Modelling collision speed in case of a crash	67
6.1.3	Test results chosen	68
6.1.4	Injury risk functions	69
6.1.5	Estimation of the posterior benefit	69
6.2	<i>Extrapolation</i>	70
6.3	<i>Sensitivity analysis</i>	71
6.4	<i>Market penetration</i>	76
7.	Discussion and conclusions	78
	Bibliography	80



List of figures

Figure 1: The preliminary safety impact assessment framework for SAFE-UP as defined in D5.1.....	14
Figure 2: Pedestrian fatality risk $P(K)$ and KSI risk $P(KSI)$	20
Figure 3: Cyclist fatality risk $P(K)$ and KSI risk $P(KSI)$	20
Figure 4: The three baseline approaches, image taken from (ISO/TR 21934, 2021) (under development).....	22
Figure 5: Process for re-simulation of GIDAS-PCM accidents in IPG CarMaker.	23
Figure 6: Example PCM-case import in IPG CarMaker.....	23
Figure 7: Reference scenarios for Demo 4 pedestrian baseline cases, taken from D3.7, figure 2.....	24
Figure 8: GIDAS Filters for Demo 4 pedestrian baseline cases.....	25
Figure 9: Reference scenarios for Demo 4 bicyclist baseline cases, taken from D3.7, figure 3.	25
Figure 10: GIDAS Filters for Demo 4 pedestrian baseline cases.....	26
Figure 11: Overview of conflict scenarios for car to pedestrian crashes – schematic representation (taken from D2.6 (Bálint, Labenski, et al., 2021)). Use-cases selected for consideration for Demo 4 are marked by the red boxes.	27
Figure 12: Overview of conflict scenarios for car to cyclist crashes – schematic representation (taken from D2.6 (Bálint, Labenski, et al., 2021)). Use-cases selected for consideration for Demo 4 are marked by the red boxes.	28
Figure 13: Histogram of initial velocity values for the passenger car in the use-case P-CRwSO. The green bars represent more than 80% of the cases.....	30
Figure 14: Coordinate system of the crossing scenarios. The VuT always moves in positive x-direction, while the VRU moves in y-direction (depending on CR or CL scenarios). SO depicts the sight obstruction.....	32
Figure 15: Coordinate system of the turning scenarios TurnL-SD.....	33
Figure 16: Initial female (left) and male (right) occupant upright, reclined (top) and lean forward positions (bottom).....	37



Figure 17: Acceleration and velocity time history of selected crash pulses..... 37

Figure 18: Strain based rib (left) and lumbar spine (right) fracture assessment..... 38

Figure 19: HIC15 (left) and BrIC (right) AIS3+ injury risk curves (Craig et al., 2020)..... 39

Figure 20: Rib (left) (Iraeus & Lindquist, 2021) and lumbar spine (right) (T5.2) fracture risk curves for a 50-years-old 40

Figure 21: Dose response method exemplified for one system and one scenario..... 41

Figure 22: IPG CarMaker visualization of VRU and vehicle model vehicle architecture idealization approach 2. 47

Figure 23: FOV of investigated radar (top) and camera (bottom) sensor at dry and rainy conditions in Cartesian coordinates (left) and polar coordinates (right), taken from D3.5, figure 23..... 48

Figure 24: Camera object visibility in over rain rates in various orientations to the sensor at 0° azimuth..... 49

Figure 25: Radar object visibility in over rain rates in various orientations to the sensor at 0° azimuth. 49

Figure 26: Schematic of the co-simulation set-up. 52

Figure 27: Vehicle geometry used for collision detection. The vehicle front is on the right side of the Figure..... 53

Figure 28: VRU geometries EPTa (left) and EBT (right) (Euro NCAP, 2022b)..... 53

Figure 29: Schematic representation of the sensor field of view..... 54

Figure 30: High level interaction layouts between Demo 3 functionalities. Subsystems relevant for the simulations are marked in light blue (Löffler, Gloger, et al., 2022). 55

Figure 31: Interfaces between the Virtual Vehicle ModelCONNECT framework and the Demo 3 ROS2 framework. 56

Figure 32: Impression from Demo 3 physical testing. 56

Figure 33: Vehicle technology architecture (from D3.9) in comparison to simulation architecture..... 61

Figure 34: Demo 4 vehicle architecture idealization approach 2. 62

Figure 35: Vehicle geometry contour. The vehicle front is on the right side of the Figure. 63



Figure 36: Field of View of Near Range Sensor (NRS) and the Far Range Sensor (FRS) the sensors fitted in the real vehicle..... 64

Figure 37: Representation of some of the parameters of the Object 3D sensor utilized in the simulations..... 64

Figure 38: Crash distribution of the main crash type categorised based on weighted IGLAD data. The weights based on location, and accident severity 73

Figure 39: Crash distribution of the main crash type categorised based on weighted IGLAD data. The second set of weights based on location, light condition and accident severity. 74

Figure 40: Crash distribution of the main crash type categorised based on weighted IGLAD data. The third set of weights based on location, weather condition and accident severity. 75

List of tables

Table 1: Injury risk functions for head and neck injury criteria 16

Table 2: Injury risk function for thorax and abdomen injury criteria for frontal and lateral loading 16

Table 3: Injury risk functions for pedestrians, based on kinematic quantities..... 18

Table 4: Injury risk functions for cyclists, based on kinematic quantities..... 19

Table 5: SAFE-UP use-cases and the corresponding Euro NCAP test cases that serve as template for scenario definition. 28

Table 6: Parameters for TurnL-SD..... 32

Table 7: Simulation matrix..... 35

Table 8: Positioning angles. 36

Table 9: Dimensions of CM-models..... 47

Table 10: Ranges for the initial velocity to be simulated for each individual car-to-pedestrian use-case (C2P)..... 51

Table 11: Ranges for the initial velocity to be simulated for each individual car-to-bicycle use-case (C2B)..... 51



Table 12: Ranges for the initial velocity to be simulated for each individual use-case (C2P). 60

Table 13: Ranges for the initial velocity to be simulated for each individual use-case (C2B). 60

Table 14: Ranges for the initial velocity simulated for each individual use-case (C2P) by IDIADA. 60

Table 15: Ranges for the initial velocity simulated for each individual use-case (C2B) by IDIADA. 60

Table 16: Matching of test scenarios and use cases. 69

Table 17: Weighting factors between IGLAD and CARE for the first set of variables. 72

Table 18: Weighting factors between IGLAD and CARE for second set of variables. 73

Table 19: Weighting factors between IGLAD and CARE for third set of variables. 74

Table 20: Overview of different crash types and the expected changes in the crash type distribution based on an analysis of weighted IGLAD data. 76

Table 21: Examples of fleet penetration rate for AEB systems for VRUs. 77



List of abbreviations

Abbreviation	Meaning
AF	Added Feature Restraint System
AV	Autonomous Vehicles
AES	Autonomous Emergency Steering
AEB	Autonomous Emergency Braking
AD	Autonomous Driving
AIS	Abbreviated Injury Score
B-CL	Bicyclist Crossing from Left
B-CR	Bicyclist Crossing from Right
B-CLwSO	Bicyclist Crossing from Left with Sight Obstruction
B-CRwSO	Bicyclist Crossing from Right with Sight Obstruction
B-PCTurnL	Bicyclist in conflict with Passenger Car Turning Left
BRIC	Brain Injury Criterion
CARE	EU Community database on road crashes, including data from police-reported crashes in EU and EFTA member states and the United Kingdom
CA	Consortium Agreement
CAV	Connected Automated Vehicles
C-ITS	Cooperative Intelligent Transport Systems
CSDM	Cumulative Strain Damage Measure
CTI	Combined Thoracic Index
D	Deliverable within SAFE-UP (e.g., D5.8 denotes SAFE-UP deliverable 5.8)
Demo	SAFE-UP demonstrator (e.g., Demo 2 denotes SAFE-UP Demonstrator 2)
EC	European Commission
EU	European Union, including the member states in 2021
GA	Grant Agreement
GIDAS	German In-Depth Accident Study
FOV	Field of view
HIC15, HIC36	Head Injury Criterion, computed on a 15ms or 36ms sliding time frame
KSI	Killed or severely injured
MAISx+	Maximum AIS score of all body parts, graded x or higher (e.g. MAIS3+)



Nij	Neck Injury Criterion
NRS	Near Range Sensor
FRS	Far Range Sensor
OEM	Original Equipment Manufacturer
OBU	On Board Unit
PCB	Printed Circuit Board
PMHS	Post mortem human subjects
P-CLwSO	Pedestrian Crossing from Left with Sight Obstruction
P-CRwSO	Pedestrian Crossing from Right with Sight Obstruction
P-PCTurnL	Pedestrian in conflict with Passenger Car Turning Left
RSU	Road-site Unit
SOTA	State-of-the-Art
T	Task within SAFE-UP (e.g., T5.3 denotes SAFE-UP task 5.3)
TTI	Thoracic trauma index
T12-Y	Lateral acceleration of the 12 th vertebra
VCmax	maximum of the product of velocity of chest deformation (V) and compression (C)
V2X	Vehicle-to-Everything
VRU	Vulnerable road user
VuT	Vehicle under test
WP	Work Package within SAFE-UP (e.g., WP5 denotes SAFE-UP work package 5)



1. Introduction

The aim of task T5.3: ‘Method development for impact assessment for Demos 1-4’ is to develop the methods that will be used for the impact assessment of each safety system (Demos 1-4). The assessment method for each Demo highly depends on the developed systems and their ability to be assessed virtually and/or physically. When possible, combinations of both approaches are considered.

A general framework for assessing the safety benefit of the SAFE-UP safety technologies was proposed in SAFE-UP Deliverable D5.1 (Mensa et al., 2021), see Figure 1. Work in T5.3 has been directed towards understanding and implementing the various elements of the framework (i.e., the boxes in Figure 1 as well as the connections between the boxes). Deliverable 5.2 has been published describing the initial work of the task and the initial methodology. This deliverable, D5.8, is describing the final methodology for safety benefit assessment.

The developed methodology is described in this deliverable, while the results of the implementation of the method are reported in Deliverables D5.3, D5.4, and D5.6 in T5.4

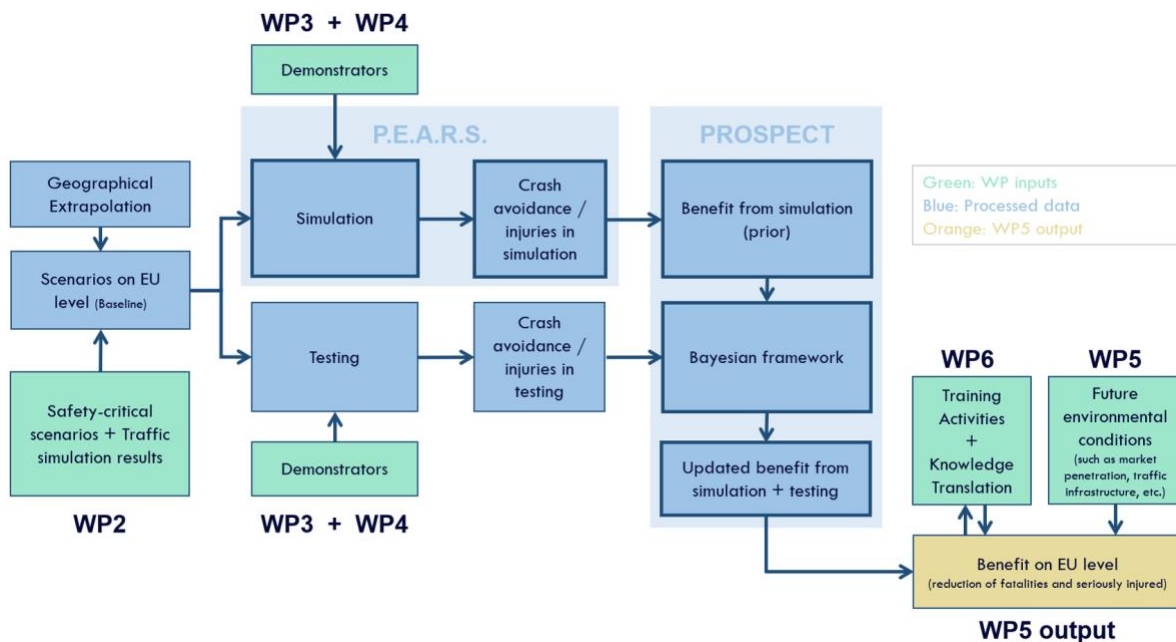


Figure 1: The preliminary safety impact assessment framework for SAFE-UP as defined in D5.1.

As noted in D5.2, the relevant assessment activities may differ between Demos. Therefore, the sections in this deliverable are organized as follows. Section 1 includes background information relevant for the several Demos, such as literature review on injury risk functions, baseline definition method and technical aspects of the implementation of the use-cases. Sections 2-5 are demonstrator-specific, addressing Demos 1 to 4, respectively. Each of these sections begins with brief overview of the safety technologies included in the corresponding Demo, followed by the details of the virtual simulations and physical testing



that have been performed or are planned (activities done in parallel of the writing of this deliverable) to assess the safety benefit of the technologies included in the Demos. Section 6 deals with the aspects that apply to several Demos at the same time, as detailed above. This deliverable ends in Section 7 with discussion and conclusions.

1.1 Literature review on injury risk functions

When simulating or physically testing safety systems in traffic scenarios, physical kinematic quantities will be the immediate results, such as the speed of the VuT at the impact or the accelerations measured in certain locations of crash test dummies. Those quantities cannot be used directly to estimate the benefit of safety systems in terms of injury or fatality risks. Therefore, Injury risk functions (IRFs) are required. IRFs provide a relationship between kinematic quantities and allow to compute probabilities to suffer various types of injuries. Such IRFs are used in SAFE-UP to achieve a meaningful estimate for the potential reduction in killed and severely injured road users. An extensive literature review has been conducted to list relevant IRFs, with a priority on:

- IRFs that are used to define thresholds in NCAP protocols.
- IRFs that are newer and/or based on the larger data set when several IRFs are available for a specific type of kinematic quantity, collision configuration and injury type.

The following sections focus on IRFs that assess the risk to suffer an injury in specific body parts and the risk to suffer injuries anywhere on the body based on collision parameters in in Section 1.1.1 and Section 1.1.3, respectively.

1.1.1 Injury risk functions to assess individual body parts

The IRFs for head and neck injury criteria are shown in Table 1, while the IRFs for thorax and abdomen are shown in Table 2. In those tables, the column “Region” refers to the body region to which the potential injuries belong, while “Injury criterion” refers to the abbreviation of the criterion name, as denoted in the literature. The full-length names of the criteria can be found in the list of abbreviations at the beginning of this document. The injury type refers to the rating on corresponding injury risk scales, such as the AIS scale. The column “Reference” lists the publication where the IRF is developed, “Case #” shows how many data points were used to establish the IRF and “Datatype” briefly describes the origin of the data points. “PMHS” refers to tests with Post mortem human subjects, where cadavers or parts of cadavers were used to determine the response of the human body to certain load cases.



Table 1: Injury risk functions for head and neck injury criteria

Region	Injury criterion	Injury type	Reference	Case #	Datatype
Head	HIC15	AIS4+, AIS5+	(NHTSA, 2000) (Prasad & Mertz, 1985)	54	PMHS: head drop tests, sled tests
	HIC36	AIS4+, AIS5+	(NHTSA, 2000)	HIC15 \approx 0.7*HIC36	
	HIC15	AIS2+, AIS3+	(Craig et al., 2020)	Summary of several publications	
	BRIC	AIS4+, AIS5+	(Takhounts et al., 2011)	114	Football player data, animal tests
	BrIC	AIS4+, AIS5+	(Takhounts et al., 2013)	114	Football player data, animal tests
	CSDM	AIS4+	(Takhounts et al., 2011)	114	Animal tests, FE simulations
	BrIC	AIS1+, AIS2+, AIS3+, AIS4+, AIS5+	(Craig et al., 2020)	Summary of several publications	
	Further Head IRFs outside of AIS scale: HIP (MTBI), PI (subdural hematoma), PRHIC/RIC (MTBI), KLC (concussion), SFC (skull fracture)				
Neck	Nij	AIS4+, AIS5+	(R. Eppinger et al., 1999) (Willinger et al., 2020)	15	Animal tests

Table 2: Injury risk function for thorax and abdomen injury criteria for frontal and lateral loading

Region	Injury criterion	Injury type	Reference	Case #	Datatype
Thorax (Frontal)	Deflection, Compression	AIS4+, AIS5+	(R. Eppinger et al., 1999; Viano & Lau, 1988)	63, 37	Frontal impact sled tests, blunt frontal impacts (PMHS)
	Max. 3ms clip of spinal acceleration	AIS4+, AIS5+	(R. H. Eppinger, 1989) (R. Eppinger et al., 1999)	63	Frontal impact sled tests (PMHS)
	Vcmax	AIS4+	(Viano & Lau, 1985, 1988)	37	blunt frontal impacts (PMHS)



	CTI	AIS4+, AIS5+	(R. Eppinger et al., 1999; R. H. Eppinger, 1989; Thompson, 2008)	63	Frontal impact sled tests (PMHS)
Thorax (Lateral)	Deflection, Compression	AIS4+	(Viano, 1989)	15	Blunt lateral impacts (PMHS)
	VCmax	AIS4+	(Viano, 1989)	15	Blunt lateral impacts (PMHS)
	Max-rib TTI, R4-scaled TTI, T12Y, Upper sternum accel, ASA10, Fmax	AIS4+	(Cavanaugh et al., 1993)	17	Lateral sled tests (PMHS)
	TTI	AIS4+, AIS5+	(R. H. Eppinger et al., 1984)	49	Mixed
	T8-Y (max. lat. Acc. of T8)	AIS4+	(Viano, 1989)	15	Blunt lateral impacts (PMHS)
Thorax	Max. rib strain per rib	Fracture risk	(Iraeus & Lindquist, 2021)	Based on (Kemper et al., 2005, 2007)	
	Max. rib strain in all 24 ribs	Number of fractured ribs NFR1+ (AIS1+) NFR2+ (AIS2+) NFR3+ (AIS3+)	(Forman et al., 2012)	133	Frontal collision
Abdomen (Frontal)	Vcmax	AIS4+, AIS5+	(Lau & Viano, 1986; Viano & Lau, 1988)	20	blunt frontal impacts (swine)
Abdomen (Lateral)	Deflection, Compression	AIS4+	(Viano, 1989)	14	Blunt lateral impacts (PMHS)
	VCmax	AIS4+	(Viano, 1989)	14	Blunt lateral impacts (PMHS)
	T12-Y	AIS4+	(Viano, 1989)	14	Blunt lateral impacts (PMHS)



1.1.2 Selection of injury risk functions: occupant injury assessment

The selection of injury risk functions for occupant injuries is described in Section 2.3.

1.1.3 Injury risk functions based on crash parameters

This section describes the IRFs, found in the literature, based on crash parameters such as impact speed, VRU age, or type of VRU. A summary of the IRFs for pedestrians is shown in Table 3, while the IRFs for cyclist are listed in Table 4. In the tables below, the column “Metric” describes the kinematic quantity that is linked by the IRF to an injury risk. “Prediction type” describes which type of injury is being predicted. In this column, KSI refers to “Killed or severely injured”, ISSx to a specific “Injury severity score” x, MAISx+ to a maximum AIS (abbreviated injury score) over all body parts of x or higher. The addition “+F” refers to a certain MAISx+ grade or a fatality. The “reference” column lists the publications where the IRF is developed, the “impact configuration” column describes the accident type for which the IRF is valid and “Case #” describes the number of data points used to establish the IRF. Further parameters might often include for example the age of the impacted VRU. Furthermore, a different version of the IRF might be used depending on whether the VRU was an elderly person, an adult or a child.

Table 3: Injury risk functions for pedestrians, based on kinematic quantities.

Metric	Prediction type	Reference	Impact configuration	Case #	Further parameters
Impact speed	Fatality	(Rosén & Sander, 2009)	Ped. Hit by veh. Front	490 cases, 36 fatalities	Age
Squared speed	Slight, Severe, Fatal	(Cuny et al., 2018)	Ped. Hit by veh. Front	(5000+): 3097/1871/195	-
Impact speed	Fatal	(Hussain et al., 2019)	Ped. Hit by veh. Front	Metaanalysis of 20 studies	Age, year, etc.
Impact speed	KSI, Fatal	(Saadé et al., 2020)	Ped. Hit by veh. Front	901/106	Age
Impact speed	ISSx	(Niebuhr et al., 2013)	Ped. Hit by veh. Front	852	-
Impact speed	MAIS2+, MAIS3+	(Spitzhuettl & Liers, 2016)	Ped. Hit by veh. Front	156 cases, 43/19 MAIS2+/3+	-
Impact speed	MAIS3+F	(Niebuhr et al., 2016)	Ped. Hit by veh. Front	1194 cases, 209 MAIS3+F	Elderly, Child. Adult, all



Table 4: Injury risk functions for cyclists, based on kinematic quantities.

Metric	Prediction type	Reference	Impact configuration	Case #	Further parameters
Impact speed	Fatality, MAIS3+F	(Rosén, 2013)	Cyclist hit by veh. front	607 (43 AIS3+F, 8 fatality)	-
Impact speed	Slight, Severe, Fatal	(Chajmowicz et al., 2019)	Cyclist hit by veh. front	643/383/53	-

1.1.4 Selection of injury risk functions: frontal crashes with VRUs

1.1.4.1 Vehicle to pedestrian crashes

The criteria to choose the appropriate IRF among those that were available are the following:

- Case number used to establish the IRF should be as large as possible
- The input kinematic quantity should be an easily obtainable result of the physical tests or simulations, such as the impact speed
- The impact configuration in the data points used to establish the IRF should correspond to the impact configuration investigated in the use-cases.

Since all use-cases for Demo 2, 3 and 4 involve frontal impacts, the chosen IRF should be valid for such impacts. Based on the literature review listed in Table 3, on the above mentioned criteria, the IRFs in (Cuny et al., 2018) were chosen to model the probabilities for pedestrians to be killed ($P(K)$) or to be killed or severely injured ($P(KSI)$), i.e., $P(K) \leq P(KSI)$. Those probabilities are expressed in dependence of the impact speed v_c (provided in kph) and they are valid for frontal crashes:

$$P(K) = 1 - \exp(-\exp(-4.6451 + 0.00079 * v_c^2))$$

$$P(KSI) = 1 - \exp(-\exp(-1.5174 + 0.00079 * v_c^2))$$



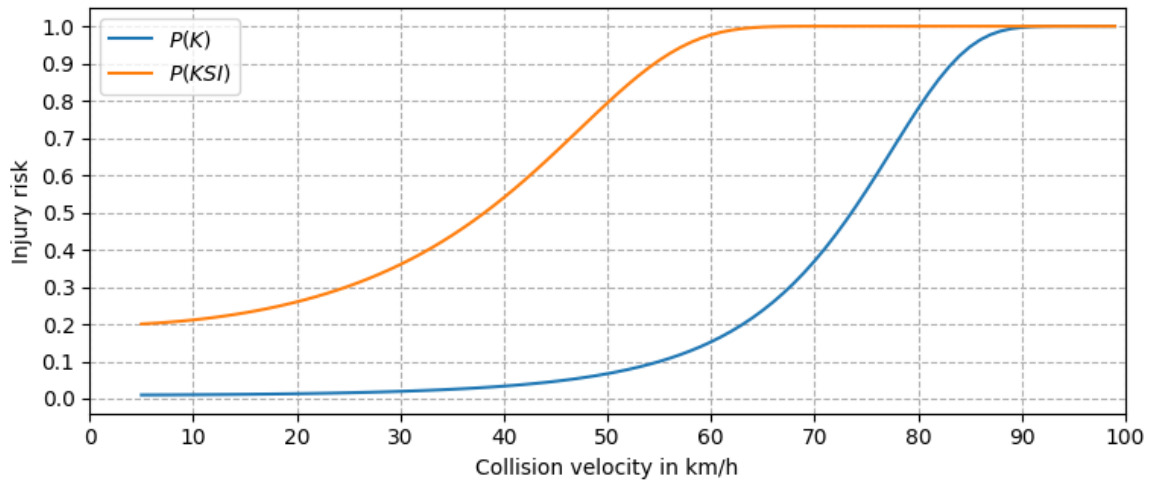


Figure 2: Pedestrian fatality risk $P(K)$ and KSI risk $P(KSI)$.

1.1.4.2 Vehicle to cyclist crashes

Analogous to the IRFs for pedestrian crashes, and due to the application of the same criteria, the IRFs in (Chajmowicz et al., 2019) for vehicle to cyclist crashes were chosen (see Table 4):

$$P(K) = 1 - \exp(-\exp(-4.6998 + 0.000799 * v_c^2))$$

$$P(KSI) = 1 - \exp(-\exp(-1.6296 + 0.000799 * v_c^2))$$

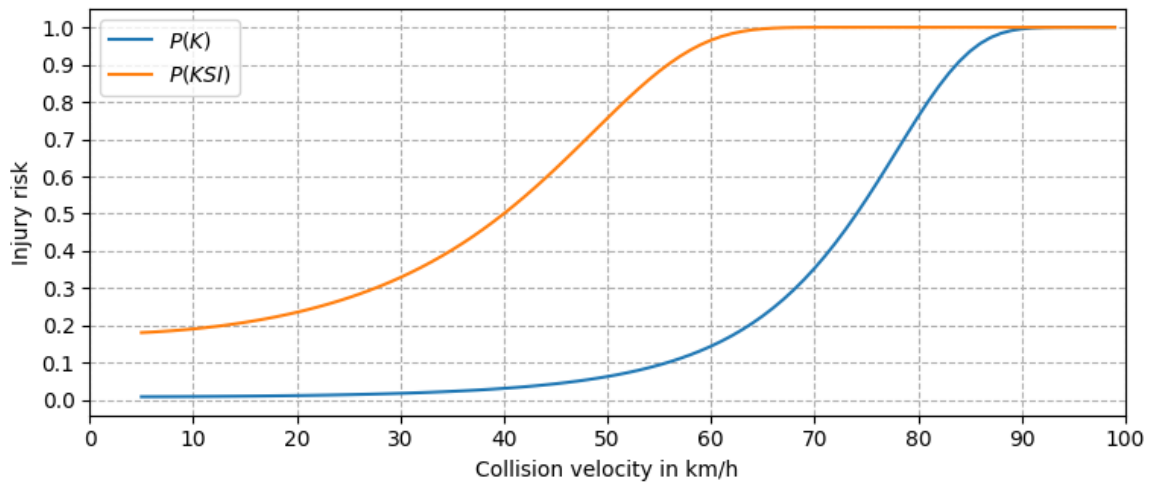


Figure 3: Cyclist fatality risk $P(K)$ and KSI risk $P(KSI)$.



1.2 Baseline definition method

According to P.E.A.R.S and the pre-defined framework (Figure 1), there are multiple ways of defining a baseline. These methods include approach A, where real accidents represented by numerical time-series data are directly resimulated. Approach B extends approach A by introducing a modification of the real world accident scenarios, for example by exchanging the vehicle model or introducing precipitation. Approaches C1 and C2 require analysis of crash mechanisms to generate synthetic cases. With C1, trajectories are pre-defined and is used when fewer cases are required, while for C2, the trajectories are generated by in-simulation models such as vehicle and trajectory following models. Approach C2 is applicable when high case numbers are required ((ISO/TR 21934, 2021), under development)

For Demo 2 and Demo 4, baseline approach B was chosen. The correlation of real world accidents to the developed technologies show exactly the performance in a wide range of really happened accidents. This variability includes environmental effects (road friction, driver visibility), VRU-behaviour and driver behaviour. Furthermore, the accident data and its relation to all accidents happened within a database, can be used to extrapolate to other databases. For the specific research question of Demo 2 real happened accidents in adverse weather can be assessed, with all relevant influencing factors and for Demo 4 the interaction and individual behaviours of the assessed VRU-crashes can be taken into account.

For Demo 3, baseline approach C2 was used since it allows to provide a large number of individually differing scenarios by variation of scenario parameters that might possibly influence the effectiveness of the technology under test, and it is initially not clear what the most important parameters are. By applying uniform variation, it can be ensured that a large range of possible parameter combinations that occur in real accidents are covered. For parameters such as traffic participant velocities, where a distribution is available from analysis of in-depth accident databases, a weighting is applied in the final computation of the effectiveness metrics.

In the following sections, the two applied P.E.A.R.S. (Page et al., 2015) baseline approaches (Figure 4) are described, since they have been used for Demo 2, 3 and 4.



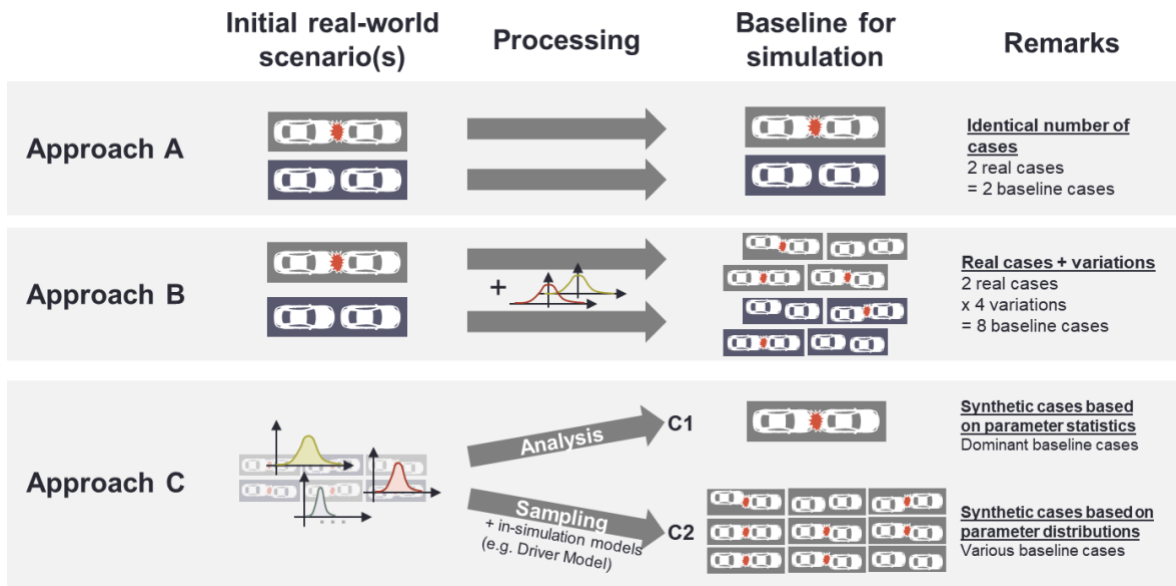


Figure 4: The three baseline approaches, image taken from (ISO/TR 21934, 2021) (under development).

Baseline approach B, which is a representant for real-world reconstructed accidents with modifications and baseline approach C2 which represents a variation of scenarios based on statistical values from accident data. The benefit of approach B is mainly that the technology can be tested on real-world accidents, whereas approach C2 brings a more general view on the technology performance.

1.2.1 Baseline definition, Approach B

As already stated, the approach followed by baseline B is a scenario set, based on real-world reconstructed accidents, which are modified in that way, that the baseline is not the initial real-world accident as reconstructed but changed by e.g., specific environmental effects or a vehicle technology (AEB, ABS), which was not present in the original crash case. In D2.6, a detailed GIDAS accident study, including a description of the applied filters, was performed to retrieve relevant scenarios for the different application areas of the Demo 2 and Demo 4. A sub-set of reconstructed accidents are available in the so called GIDAS Pre Crash Matrix (GIDAS-PCM). In this study the GIDAS-PCM cases are imported in IPG-CarMaker for resimulation and creation of a baseline, see Figure 5.





Figure 5: Process for re-simulation of GIDAS-PCM accidents in IPG CarMaker.

The PCM Importer imports the relevant road markings, objects and target (T00) trajectories (see Figure 6). The ego-trajectory will be imported as “follow-route” maneuverer. This enables the vehicle to still act with its defined vehicle dynamics physically correct. But it needs to be noted, that this approach leads to a slightly different collision pose compared to the reconstructed accident, since it is not always possible to follow the predefined trajectory.

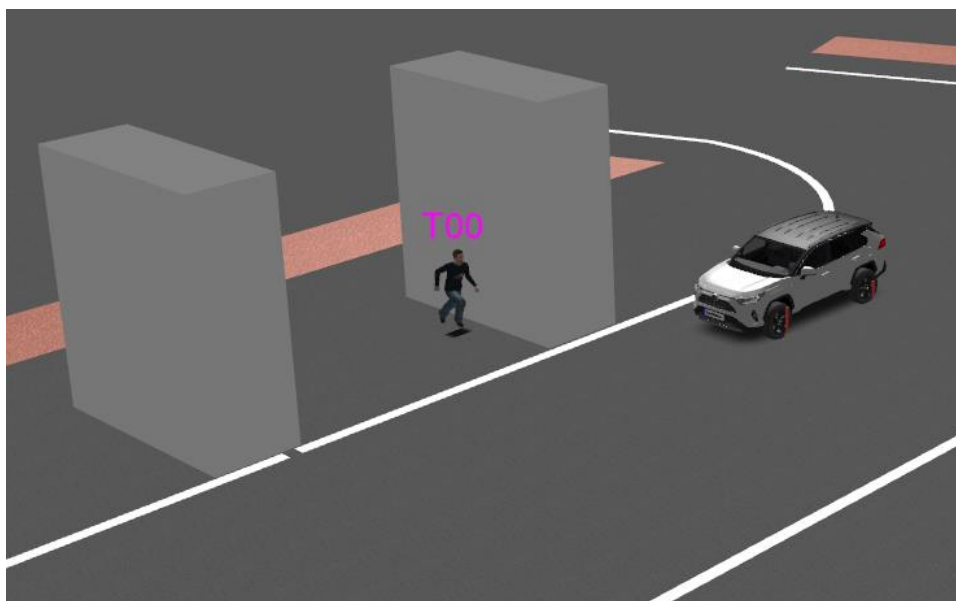


Figure 6: Example PCM-case import in IPG CarMaker.

1.2.1.1 Approach B for Demo 2

For Demo 2 relevant scenarios for the assessment are defined in D2.6, section 4.3.4.3. The GIDAS-PCM-Cases for the pedestrian scenarios P-CLwoSO (Pedestrian crossing left without sight obstruction) and P-PCTurnL (Passenger car turning left) are the reference for the creation of the baseline. The GIDAS-PCM-Cases for the B-CR (Cyclist crossing from right while PC moves forward) and B-PCTurnL (Cyclist in conflict with PC turning left) scenarios are the reference for the baseline of the bicyclist cases. The applied modification



for the baseline is, that for all cases the reconstructed weather conditions will be used to modify the sensor FOV for the applied sensor set. . The precipitation will have influence on the sensor FOV performance and the underlying friction coefficient. Furthermore, the baseline model will get included a TTC-based AEB system (see 1.2.1.3).

1.2.1.2 Approach B for Demo 4

For Demo 4 relevant scenarios are described in In D3.4 (Nikolaou et al., 2021), Section 4.2.1. Figure 7 and Figure 9 show those scenarios where a C-ITS System is expected to provide a benefit compared to today. P-PCTurnL and P-CRwSO PCM-Cases are the reference scenarios for the baseline creation for the pedestrian cases. B-CR, B-CL and B-PCTurnL PCM-Cases are the reference scenarios for the bicyclist cases. The baseline will consider all B-CR and B-CL PCM-cases and not just the obstruction cases. Thus, a benefit assessment of the C-ITS system in non-obstructed cases with higher cyclist speeds will also be enabled. The GIDAS-PCM only includes first collision accidents, so no further filtering on single causing accidents needs to be done.

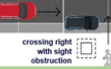
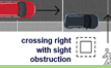

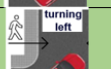
Scenario ID	VRU Type	D2.6 scenario label	Pictogram	Injury coverage		Speed (Km/h)				Total test cases
				% KSI	%All	VUT (KSI/All)	VUT (Proposal)	VRU (KSI/All)	VRU (Proposal)	
Demo_4_01	Pedestrian	C-ITS-P3 D2.6 P-CRwSO		18,7	17,1	26 - 45	25 - 45 (every 5 Kph)	-	8	5
Demo_4_02	Pedestrian	C-ITS-P3 D2.6 P-CRwSO		18,7	17,1	27 - 45	35 - 65 (every 5 Kph)	N/A	5	7
Demo_4_05	Pedestrian	D2.6 P-PCTurnL		9,2	11	10 - 28	10 - 30 (every 5 Kph)	-	5	5
Demo_4_06	Pedestrian	D2.6 P-PCTurnL		9,2	11	10 - 28	10 - 30 (every 5 Kph)	-	8	5

Figure 7: Reference scenarios for Demo 4 pedestrian baseline cases, taken from D3.7, figure 2.

The applied GIDAS-Filters for the GIDAS-PCM baseline can be seen in Figure 8. This filtering results in 452 scenarios.



Demo 4_01, Demo 4_02 GIDAS Filter

UTYP:
With Sight obstruction
 No junction (423, 424, 422)
 Before junction (452, 453, 454)
 After junction (472, 473)
W/O Sight obstruction but with SICHTBV (1, 3, 4, 8)
 No junction (421, 493, 455)
 Before junction (451, 492)
 After junction (272, 274, 471)
 +
FGRI (Pedestrian direction relative to vehicle)
 Clock (Between 2 and 4)
UQFB:
Non-designated crossing:
 Except traffic lights / zebra crossing (3 & 4)
Designated crossing:
 Only traffic lights / zebra crossing (3 & 4)

Demo 4_05, Demo 4_06 GIDAS Filter

UTYP:
 221, 282, 273, 481, 491
 +
FGRI (Pedestrian direction relative to vehicle)
 Clock (Between 8 and 12)
UQFB:
Non-designated crossing:
 Except traffic lights / zebra crossing (3 & 4)
Designated crossing:
 Only traffic lights / zebra crossing (3 & 4)

Figure 8: GIDAS Filters for Demo 4 pedestrian baseline cases.


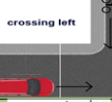
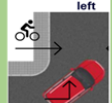
Scenario ID	VRU Type	D2.6 scenario label	Pictogram	Injury coverage		Speed (Km/h)				Total test cases
				% KSI	%All	VUT (KSI/All)	VUT (Proposal)	VRU (KSI/All)	VRU (Proposal)	
Demo_4_08	Cydist	C-ITS-B1 D2.6 B-CR + Obstruction		37,8	35,2	5-30	15-30 (every 5 Kph)	N/A	15 - 20 (every 5 Kph)	8
Demo_4_09	Cydist	C-ITS-B2 D2.6 B-CL + Obstruction		25,5	22,4	5-30	15-30 (every 5 Kph)	N/A	20	4
Demo_4_13	Cydist	D2.6 B-PCTurnL		10	17,1	11 - 29	10 - 30 (every 5 Kph)	12 - 21	15 - 20	10

Figure 9: Reference scenarios for Demo 4 bicyclist baseline cases, taken from D3.7, figure 3.

The applied GIDAS-Filters for the GIDAS-PCM baseline bicyclist cases can be seen in Figure 10. This results in 745 scenarios.



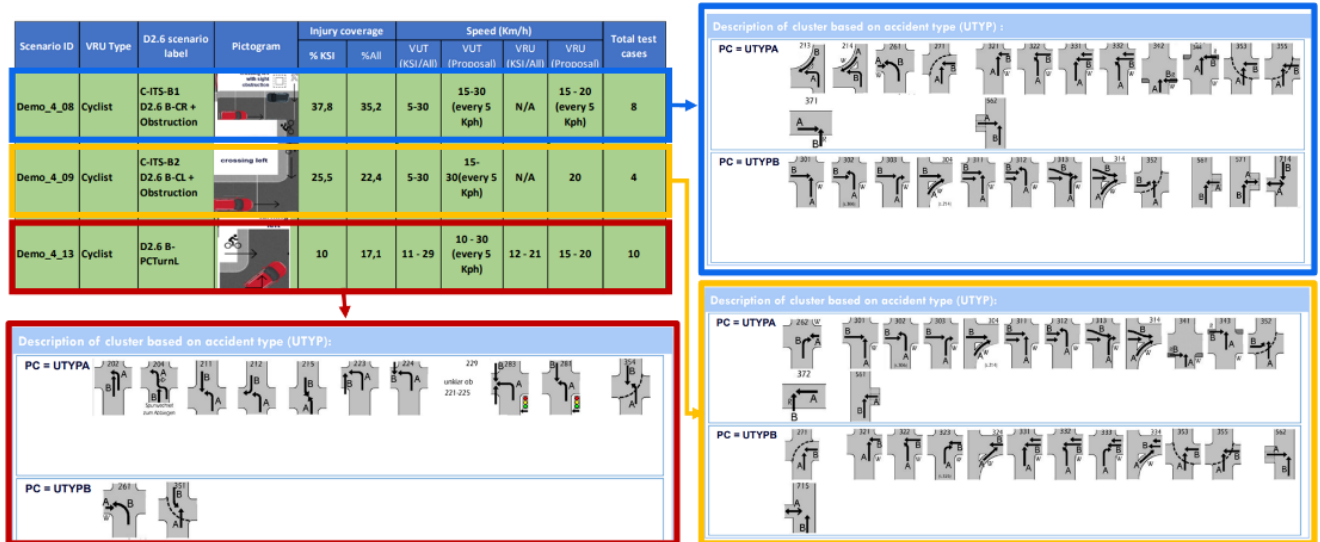


Figure 10: GIDAS Filters for Demo 4 pedestrian baseline cases.

1.2.1.3 Approach B, System modification

The GIDAS-PCM data per se are reconstructed accidents, which mostly not include Safety-Systems like AEB. The Baseline technology for Demo 2 and 4 already is an AEB-Safety System. The act-part of this Safety-System – the TTC-based triggering and deployment of the brake-system is the same for Demo 2 and 4. An almost linear jerk of 24.5 m/s^3 and a max. deceleration of 9 m/s^2 is applied for the brake-system and the TTC-based deployment is at 1 second for a relative vehicle velocity of 10kph and 1.3 seconds for a relative vehicle velocity of 60kph.

The Baseline FCW model for Demo 4 RQ2 is a standard TTC-based FCW with triggering times of 1.6 seconds at 10kph relative velocity and 2.0 seconds above 60kph. The deceleration signal of a human driver is assumed with 6 m/s^2 . The driver reaction time is defined with 1.0s.

1.2.2 Baseline definition, Approach C2

The main steps to conduct the baseline definition via approach C2 (i.e., choosing concrete scenarios to be simulated) are explained in the following subsections, in the order they are executed. This approach is applied to generate scenarios for Demo 3 and 4.

1.2.2.1 Investigated use-cases

The first step is choosing the use-cases to be considered. The results for this step in the process can be found in D3.4 (Nikolaou et al., 2021), where use-cases of interest for each Demo are listed. The selected use-cases are the following, see also Figure 11 and Figure 12:



- P-CLwSO, B-CLwSO (Demo 3 and 4): Pedestrian or bicyclist crossing from the left, with sight obstruction
- P-CRwSO, B-CRwSO (Demo 3 and 4): Pedestrian or bicyclist crossing from the right, with sight obstruction
- P-PCTurnL-SD, B-PCTurnL-SD (Demo 4): Passenger car turning left, pedestrian or bicyclist coming from the far side
- P-CLwoSO, B-CLwoSO (Demo 3): Pedestrian or bicyclist crossing from the left, without sight obstruction
- P-CRwoSO, B-CRwoSO (Demo 3): Pedestrian or bicyclist crossing from the right, without sight obstruction.

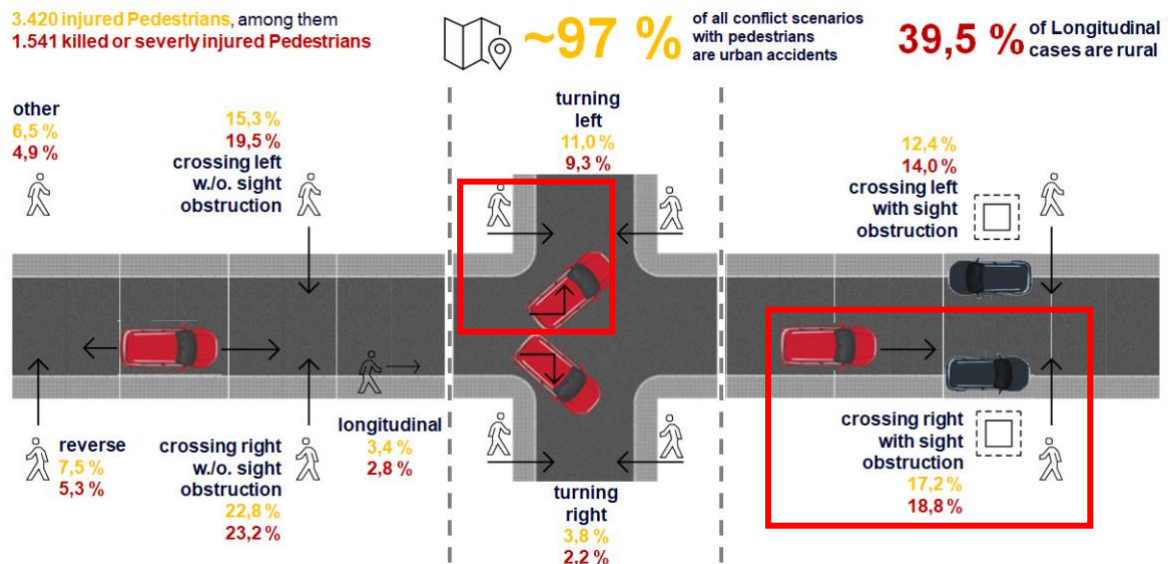


Figure 11: Overview of conflict scenarios for car to pedestrian crashes – schematic representation (taken from D2.6 (Bálint, Labenski, et al., 2021)). Use-cases selected for consideration for Demo 4 are marked by the red boxes.



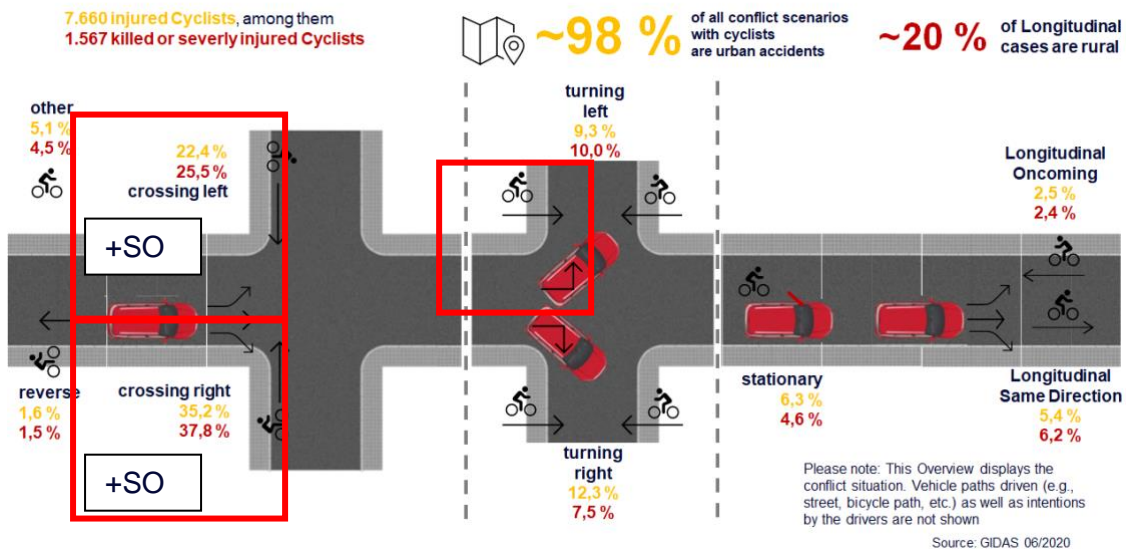


Figure 12: Overview of conflict scenarios for car to cyclist crashes – schematic representation (taken from D2.6 (Bálint, Labenski, et al., 2021)). Use-cases selected for consideration for Demo 4 are marked by the red boxes.

1.2.2.2 Defining a representative logical scenario for each use-case

For this step, an appropriate representant in the Euro NCAP (Euro NCAP, 2022b) AEB/LSS testing protocol is chosen as a template. The corresponding representants are shown in Table 5.

Table 5: SAFE-UP use-cases and the corresponding Euro NCAP test cases that serve as template for scenario definition.

SAFE-UP use-case	Corresponding Euro NCAP test case	SAFE-UP use-case	Corresponding Euro NCAP test case
P-CLwoSO	CPFA-50	B-CLwoSO	CBFA
P-CRwoSO	CPNA-25 & CPNA-75	B-CRwoSO	CBNA
P-CLwSO	CPNCO-50	B-CLwSO	CBNAO
P-CRwSO	CPNCO-50	B-CRwSO	CBNAO
P-TurnL-SD	CPTAfs	B-TurnL-SD	CPTAfs

1.2.2.3 Choosing appropriate values for the initial velocities of the VRU and VuT

For the parameters that are involved in setting up the use-cases, see Section 1.3. To define the range of variation for the VRU and VuT initial velocity parameter, a method based on a GIDAS analysis is used. For this purpose, for each use-case, the cases available in the GIDAS are filtered, such that only cases corresponding to the use-case remain. For further information on how the database cases are filtered, see D2.6 (Bálint, Labenski, et al., 2021).



For each use-case, and for the VuT and VRU respectively, a histogram of initial velocity values is derived and used to define the range velocity values that are considered. Based on the histogram, velocity bins are added to the velocity range until at least 80% of the velocity values for the respective use-case are covered, see Figure 13. The limit of 80% is chosen as a compromise between the following two arguments and led to case numbers that are feasible in simulation: on the one hand, if the full range of values that occur in the GIDAS is used, then the largest possible coverage of values that occur in real accidents can be covered. On the other hand, as the limit is increased, additional velocity bins will contain fewer and fewer cases, such that the additional gain in coverage per velocity bin decreases (see for example the bins from 66-100 kph in Figure 13), leading to large final velocity ranges and therefore to very large case numbers that become unfeasible to handle even in simulation.

As values for the velocity, the initial velocity in the GIDAS is used which is defined as the speed in km/h before a critical situation was recognised. It is the most appropriate parameter (as opposed to the collision speed) to define the scenarios, since the velocity is not influenced by the driver or VRU who reacts to the emerging conflict.



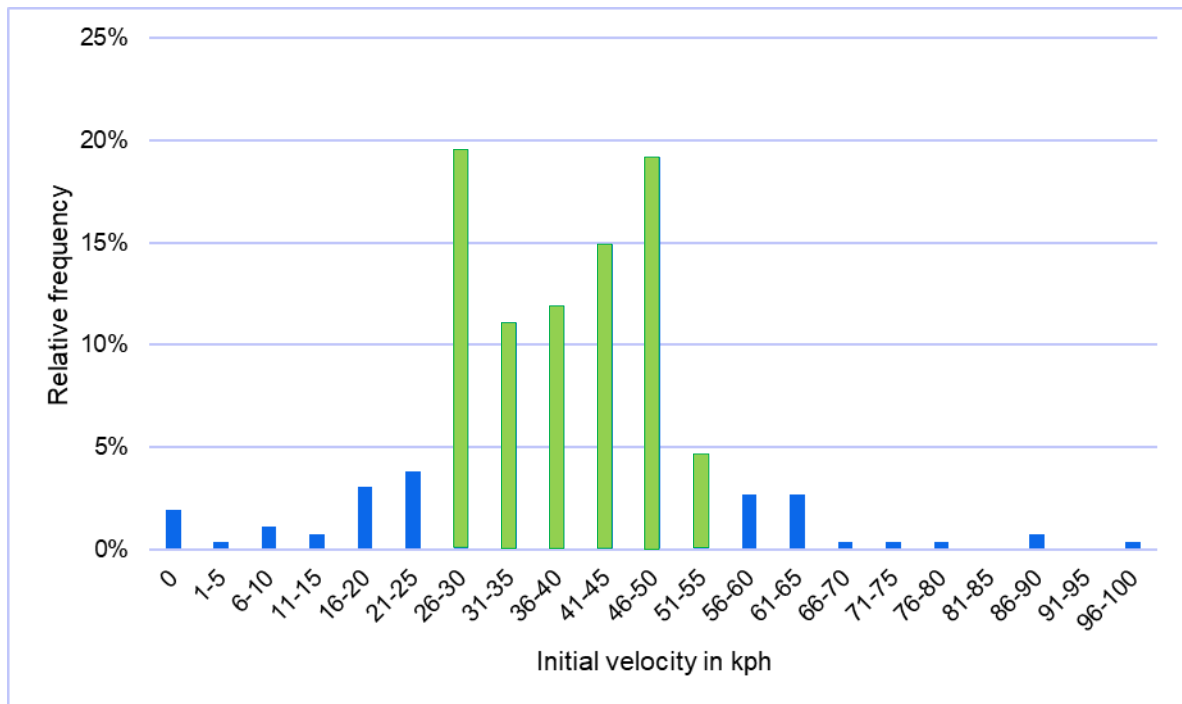


Figure 13: Histogram of initial velocity values for the passenger car in the use-case P-CRwSO. The green bars represent more than 80% of the cases.

1.3 Technical aspects of the implementation of investigated use-cases

The following section describes technical aspects for the implementation of various use-cases which are needed for the assessment of Demo 3 and 4. These use-cases are listed in Section 1.2.2.1. In particular, a parameterization of the scenarios is introduced.

1.3.1 Setup of the use-cases P/B-CLwSO, P/B-CRwSO, with and without sight obstruction

The crossing scenarios are created to take place on a straight road segment (see Figure 14). The x-axis of the global coordinate system is parallel to the road segment and is centred in the middle of the lane. The y-axis is normal to the x-axis and is defined to coincide with the edge of the VRU corridor (i.e., the space that is covered by the VRU during the scenario) with the lower x-coordinate, see Figure 14). To describe this scenario setup, the origin of the vehicle coordinate system is assumed to be the centred in its bounding box. The scenarios CPFA-50 (Car-to-Pedestrian Farside Adult) and CPNA-25/CPNA-75 (Car-to-Pedestrian Nearside Adult) in the Euro NCAP AEB/LSS testing protocol (Euro NCAP, 2022b) were used as templates, and further parameterization was introduced.



The VuT starts at the initial position x_{VuT}^{init} , y_{VuT}^{init} with initial velocity v_{VuT}^{init} , heading in positive x-direction. To allow for additional variation of the scenario, the initial position y_{VuT}^{init} is parameterized in dependence of p_{VuT}^{lat} , which is the relative lateral position within the lane, in proportion to the lane width w_{lane} (i.e., the distance between the parallel lane borders, which are located at y-positions $w_{lane}/2$ and $-w_{lane}/2$):

$$y_{VuT}^{init} = (0.5 - p_{VuT}^{lat})w_{lane}.$$

The initial x-position can then be given, using the length of the vehicle l_{VuT} :

$$x_{VuT}^{init} = -\left(t_{coll}v_{VuT}^{init} + \frac{l_{VuT}}{2}\right).$$

The VRU starts at $x_{VRU}^{init} = w_{VRU}/2$, with w_{VRU} being the width of the VRU bounding box. Since the VRU moves either in positive or negative y-direction, the x-coordinate of the VRU never changes during the scenario. As a further possibility for variation, the lateral impact position of VRU on the VuT is parameterized through p_{VRU}^{lat} . With a value of $p_{VRU}^{lat} = 0$, the y-coordinate y_{VRU}^{coll} of the VRU at the impact corresponds to the y-coordinate of the left edge of the VuT, and with $p_{VRU}^{lat} = 1$ corresponds to the right edge of the VuT:

$$y_{VRU}^{coll} = y_{VuT}^{init} + (0.5 - p_{VRU}^{lat})w_{VuT},$$

where w_{VuT} denotes the width of the VuT. While a constant velocity was chosen for VuT both for pedestrian and cyclist cases, it is assumed that the pedestrian accelerates from standstill $v_{VRU}^{init} = 0$ to its collision velocity v_{VRU}^{coll} and the cyclist moves with constant velocity $v_{VRU}^{coll} = v_{VRU}^{init}$ towards the impact location, in accordance with the EuroNCAP scenarios that were used as template, see Table 5. For the cyclist, using the heading angle ϕ_{VRU} , the initial y-coordinate can simply be calculated with by:

$$y_{VRU}^{init} = y_{VRU}^{coll} - \sin(\phi_{VRU})t_{coll}v_{VRU}^{init}.$$

It is defined that the pedestrian starts at an initial position $y_{VRU}^{init} = -4m$ for crossing from right cases and $y_{VRU}^{init} = 6m$ for crossing from left cases and then accelerates linearly with an acceleration of $a_{max} = 3 \frac{m}{s^2}$, until v_{VRU}^{init} is reached and the pedestrian continues to move with constant velocity up to the collision point. The choice of those values corresponds to the CPFA-50 (Car-to-Pedestrian Farside Adult) and CPNA-25/CPNA-75 (Car-to-Pedestrian Nearside Adult) in the Euro NCAP AEB/LSS testing protocol (Euro NCAP, 2022b).

Finally, the sight obstruction (SO) position is parameterized through the parameters D_x and D_l , where D_x denotes the distance between the sight obstruction and the VRU corridor, and D_l denotes the distance between the sight obstruction and the VuT corridor (see Figure 14). The parameter D_x is chosen as a fixed value of 3.55m for the cyclist scenarios according to the EuroNCAP protocol (Euro NCAP, 2022b), see scenario CBNAO, and 1m for the pedestrian scenarios (see EuroNCAP scenario CPNCO-50). The parameter D_l is chosen as a fixed value of 4.8m for the cyclist scenarios according to the EuroNCAP protocol (Euro NCAP, 2022b), see scenario CBNAO, and 1m for the pedestrian scenarios (see EuroNCAP scenario CPNCO-50).



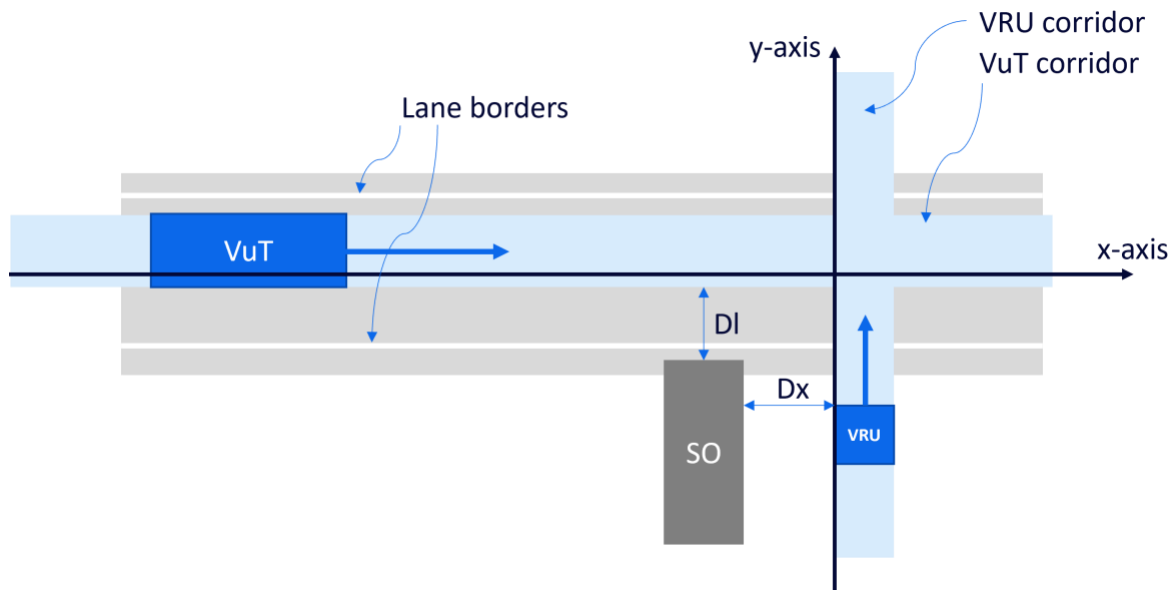


Figure 14: Coordinate system of the crossing scenarios. The VuT always moves in positive x-direction, while the VRU moves in y-direction (depending on CR or CL scenarios). SO depicts the sight obstruction.

1.3.2 Setup of the use-cases TurnL-SD

The setup of the use-case TurnL-SD is exemplified in Figure 15. This scenario is implemented in IDIADA’s simulator ASM Traffic from dSPACE platform and is described in detail in D3.7 (Nikolaou et al., 2022).

The main parameters, as given in Figure 15 are shown in Table 6.

Table 6: Parameters for TurnL-SD.

Parameter	Description
DL	Distance in y-direction between the centre of the dashed lane marking of the vehicle and VRU trajectory
DX	Distance in x-direction between the VRU initial position and the impact position (units: meters)
IWP	Target impact location on the vehicle front-bumper. It represents a point of the front-bumper starting from the right side (0%) to the left side (100%).50% represents the centre of the vehicle units: %
VS	Vehicle speed (units: kph)
VT	VRU speed (units: kph)



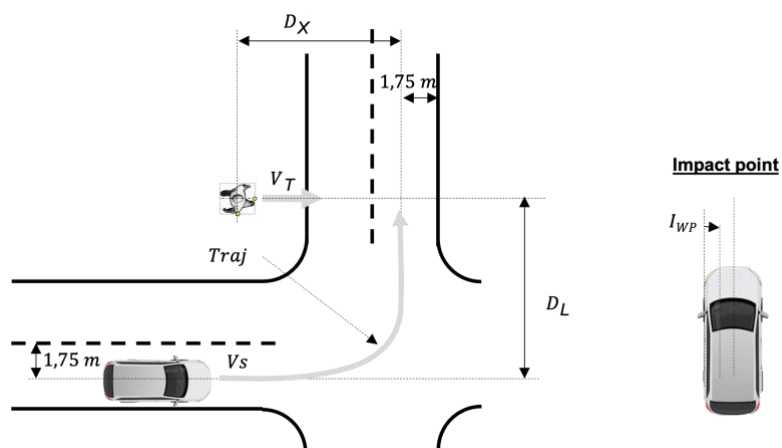


Figure 15: Coordinate system of the turning scenarios TurnL-SD.



2. Demo 1

This section describes the proposed safety assessment methodology for added-function (AF) restraint systems in Demo 1.

2.1 Workflow – Selection of crashes

Scenarios that are relevant for Demo 1 have been selected by an analysis done in WP2 D2.6 (Bálint, Labenski, et al., 2021) and WP4 D4.1 (Odriozola et al., 2021).

In-depth GIDAS data and EU data from CARE are used to calculate the safety benefit of the improved restraint passive safety systems regarding occupant injury reduction for the target region EU. The in-depth GIDAS data provide detailed information about the crashes, such as crash configurations and car-to-car crash delta velocity, deltaV, while CARE data contains fewer details on the crashes but includes data from EU countries (EC, 2019). The expectation is that the distribution of scenarios and conditions is different in CARE and GIDAS due to the different geographical regions included. While GIDAS has more detail, CARE better represents the overall EU crash distribution. Therefore, the basic approach is to use details of crashes in GIDAS as inputs to simulations and effectiveness assessment methods, but to weight those results to CARE. Weighting is accomplished using the hypercube method (D5.2), which creates weights for a small set of combinations of factors that might differ between the in-depth data and CARE. These factors are calculated based on matching variables in both datasets. (The CARE crashes from a specific year e.g., 2018 is used.) These weight factors are applied for car-to-car crashes in the in-depth data.

After weighting, the scenarios, such as car-to-car head-on crashes, which are relevant for Demo 1 restraint systems, identified in accident analysis D2.6 (Bálint, Labenski, et al., 2021) and D4.1 (Odriozola et al., 2021), are selected from in-depth crash data.

The weighted total number of the crashes in the specified scenario (e.g., car-to-car head-on) is calculated from the in-depth data. Furthermore, for these crashes (e.g., car-to-car head-on) the weighted deltaV distribution from the in-depth crash database is calculated and modelled as a lognormal distribution, $s(v)$, with the parameters μ (mean) and σ (standard deviation). In addition, injury data for the specified crash scenario, classified using the Max AIS0-6, the maximum value from the AIS injury scale ranging from 0 (not injured) to 6 (maximum) are obtained from the in-depth crash data. Specifically, the distribution of driver and occupant injuries and the distribution of the Max AIS0-6 overall injury per body region are obtained.

After the above crash data in the specific crash scenario is obtained, occupant simulations with SOTA and with the AF SAFE-UP restraint passive safety systems will be performed. These simulations are explained in the following section.



2.2 Simulations

For the safety benefit assessment of the AF restraint passive safety system in novel seating positions, occupant simulations with updated human body models (HBMs) from T5.2 will be done in T5.4.2. (Novel seating positions for the driver arise with increasing automation level and are specified in D4.1.) The respective planning was done in T5.3 and the methodology of the study setup will be described in this section.

The planned simulation study consists of 40 cases in total, including three occupant seating positions, two restraint system settings, two occupant anthropometries and four car-to-car (C2C) head-on crash severities, as shown in Table 7.

Table 7: Simulation matrix.

Seating position	Backrest angle	Restraint system	Manoeuvre	C2C head-on crashes deltaV's (kph)			
				25	40	56	75
Upright	Upright	SOTA	w/o AEB	x	x	x	x
Upright + lean forward	Upright	SOTA	w/ AEB	x	x	x	x
Upright + lean forward	Upright	Improved	w/ AEB	x	x	x	x
Reclined + lean forward	Reclined	SOTA	w/ AEB	x	x	x	x
Reclined + lean forward	Reclined	Improved	w/ AEB	x	x	x	x
Occupant model				VIVA+ F50			
				VIVA+ M50			

The finite element simulations will be done in the generic frontal system CAE model (in LS-Dyna), described in D4.4 (Becker et al., 2022) with a current state-of-the-art (SOTA) and an added-function (AF) restraint system setting.

The 50th percentile female (F50) and male (M50) occupant models (VIVA+ version 0.4.0 from T5.2) were positioned into the generic interior model for an upright and a reclined seat with backrest angles of 23° and 48° respectively and a seat pan angle of 15°. For the upright position, the occupants were positioned according to a THOR50M reference model (as it was also done in D4.4 (Becker et al., 2022)). The positioning angles can be seen in the graphic on the right in Table 8. The female and male VIVA+ models had an initial 28° sternum angle in the upright position, measured from the vertical between the jugular notch (incisura jugularis) and the lower part of the sternum (processus xiphoideus). The initial pelvis angle (α_1) was 52°, measured from the vertical between pubic symphysis and anterior superior iliac spine. For the reclined position, the initial sternum angles were (α_2) 49° and 52° and the initial pelvis angles (α_1) 74° and 79° for female and male model, which match

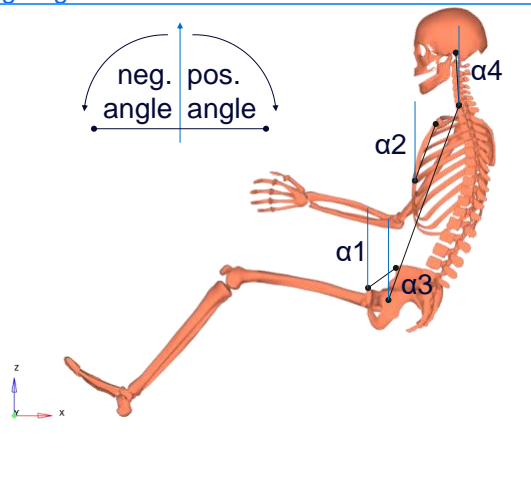


well with reclined male post-mortem-human-surrogate data (PMHS) presented in (Richardson et al., 2020).

The models were positioned from the initial upright and reclined position to lean forward positions, described by torso (α_3) and head angle (α_4) (see Table 8 (right)). These positions were predicted based on the volunteer study and the respective posture prediction model developed by VIF (in T5.2) for pre-crash manoeuvres. The selection of the lean forward positions was done for the female and male VIVA+ model based on the maximum predicted sum of the torso and head angle during automated emergency braking (AEB). Both models were positioned accordingly for the simulation of the in-crash phase and the torso and head angles for all initial positions are shown in Table 8.

Table 8: Positioning angles.

Occupant model	Seating position	Torso angle	Head angle
VIVA+ F50	Upright	27°	2°
VIVA+ F50	Upright + lean forward	15°	-15°
VIVA+ F50	Reclined	44°	22°
VIVA+ F50	Reclined + lean forward	41°	5°
VIVA+ M50	Upright	24°	2°
VIVA+ M50	Upright + lean forward	14°	-15°
VIVA+ M50	Reclined	42°	20°
VIVA+ M50	Reclined + lean forward	37°	-3°



The final occupant positions after the positioning simulations are shown in Figure 16.



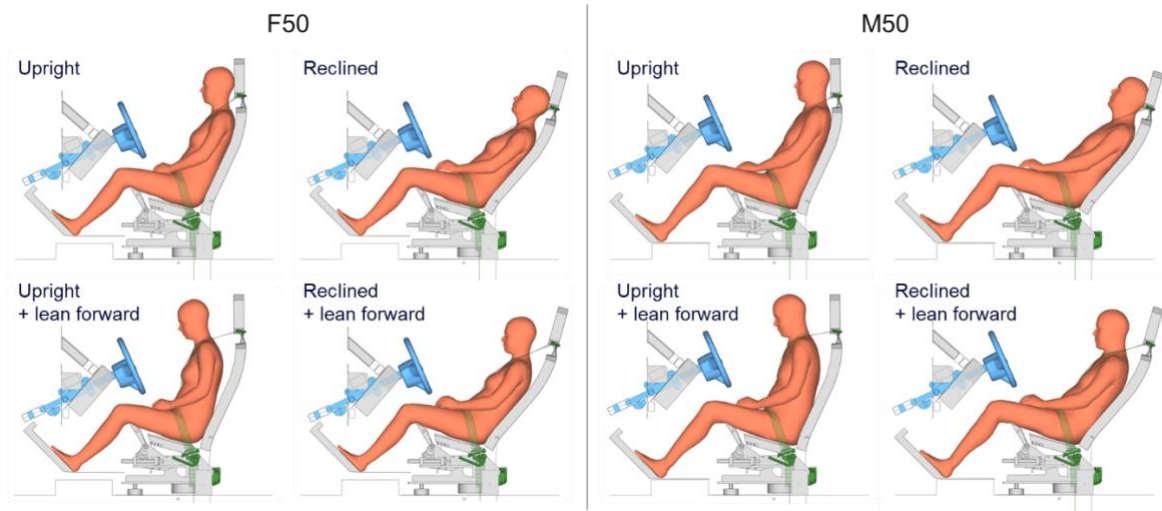


Figure 16: Initial female (left) and male (right) occupant upright, reclined (top) and lean forward positions (bottom).

The AF restraint system and SOTA restraint system will be evaluated in four load cases defined by generic crash pulses with car-to-car head-on delta velocities (deltaV's) of 25, 40, 56 and 75 kph, which are shown in Figure 17. The pulses are based on real-life frontal crashes with passenger cars and the pulse shape development was described in (Iraeus & Lindquist, 2015). According to (Iraeus & Lindquist, 2016), the following Eigenvectors were applied to create the pulses: Eigenvector 1 ($\mu = 0.57, \sigma = 1.64$), Eigenvector 2 ($\mu = -1.13, \sigma = 1.05$), Eigenvector 3 ($\mu = 0.37, \sigma = 0.74$). (For further details on the development of the pulses see reference (Iraeus & Lindquist, 2016)). In comparison to crash pulse signals, measured in real crash tests, the generic pulse signals show very little oscillation. It is not expected that this inaccuracy affects the usability of the pulses for injury assessment, as it was shown in (Iraeus & Lindquist, 2016) for chest injury prediction.

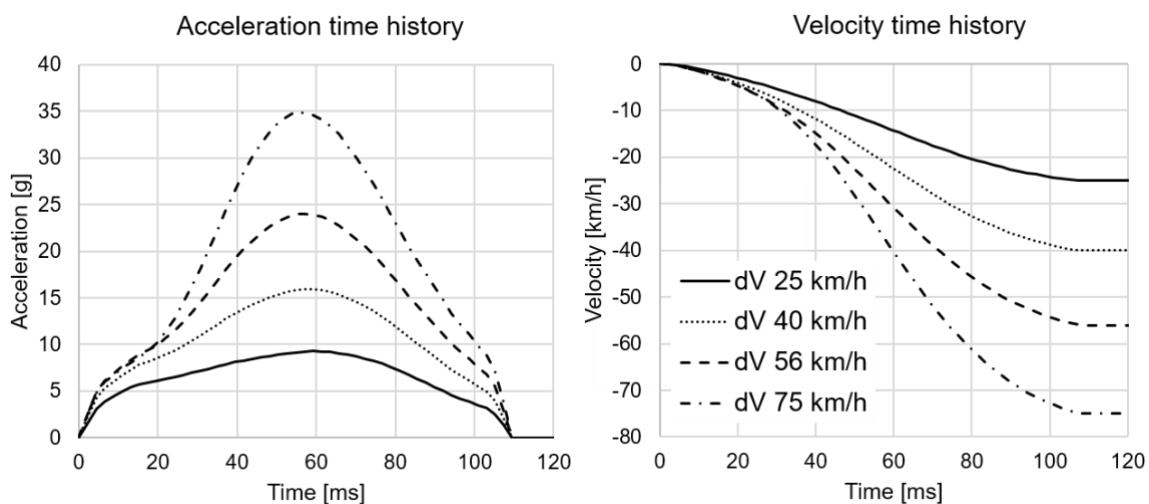


Figure 17: Acceleration and velocity time history of selected crash pulses.



The following injury mechanisms will be assessed in the model post-processing:

- Skull fracture, using the head injury criteria in a 15 ms time interval (HIC15) based on (Prasad & Mertz, 1985) and summarized in (Craig et al., 2020).
- Rotational induced brain injury, using the brain injury criteria (BrIC), based on (Takhounts et al., 2011) and summarized in (Craig et al., 2020).
- Rib fracture, based on the first principal strain in the cortical bones of the left and right ribs (Mayer C. et al., 2021) (see Figure 18).
- Lumbar spine fracture, based on the compression (superior-inferior) strain in the trabecular (spongy) bones of the vertebrae bodies (see Figure 18).
- Submarining, based on a visual inspection.

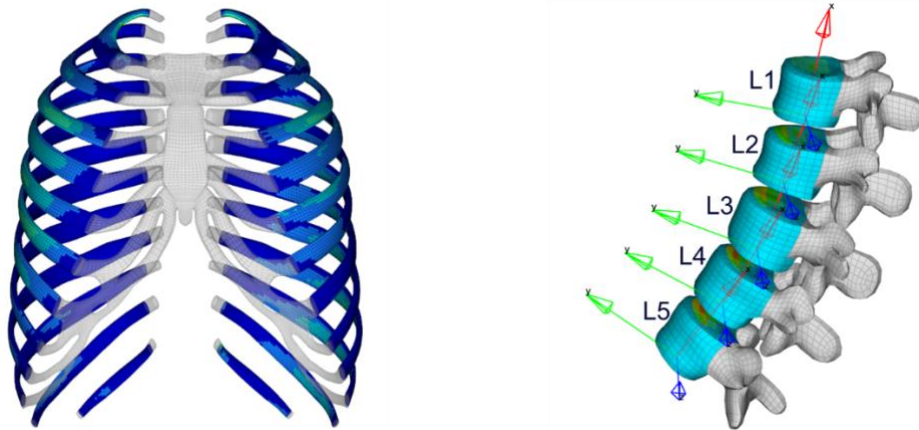


Figure 18: Strain based rib (left) and lumbar spine (right) fracture assessment.

The simulation results and evaluated criteria will function as an input to the safety benefit assessment, where AIS3+ injury risks for skull fracture, rotational induced brain injury, rib fracture and lumbar spine fracture will be calculated. The models for injury risk calculation will be described in the following chapter.

2.3 Models for injury risk probability

For the assessment of the passive safety benefits, the risk of serious injury (level 3 or higher on the abbreviated injury scale (AIS)) (AIS3+) will be assessed. To calculate the probability of AIS3+ injuries, the following injury and fracture risk curves will be applied for the head, see Figure 19, and for the lumbar spine and ribs, see Figure 20. Additionally to the rib fracture risk, the probability for at least three or more independent rib fractures (number of fractured ribs (NFR3+)) will be calculated according to (Forman et al., 2012). In this study the NFR3+ are assumed to correlate to the probability of AIS3+ injury. The rib and lumbar spine fracture risks will be calculated for a 50-years-old occupant. The lumbar spine risk was estimated from the maximum strain in any of the five lumbar vertebrae. The risk curves used to calculate risk of lumbar spine injury was constructed from reconstructions of past tests on



lumbar spine units from PMHSs. AIS levels or amount of vertebra crush were not presented in the original works. For these reasons, the injury risk estimated was for the onset of an AIS2+ injury. However, several of the specimens tested appear to be injured at AIS3 level.

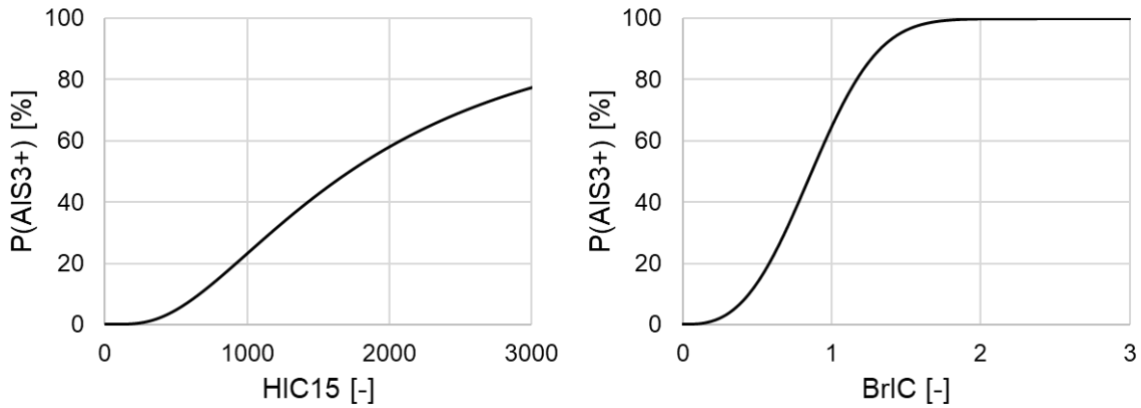


Figure 19: HIC15 (left) and BrIC (right) AIS3+ injury risk curves (Craig et al., 2020).

The related functions are listed below (including the parameter values as stated in the corresponding reference):

HIC15 (Craig et al., 2020):

$$HIC = |(t_2 - t_1) \left[\frac{1}{t_2 - t_1} \int_{t_1}^{t_2} a(t) dt \right]^{2.5}|_{max} \quad \text{for } t_2 - t_1 \leq 15 \text{ ms}$$

$$P(AIS3+) = \Phi \left[\frac{\ln(HIC_{15}) - 7.45231}{0.73998} \right] \quad \text{with } \Phi = \text{Cumulative normal distribution function}$$

BrIC (Craig et al., 2020):

$$BrIC = \sqrt{\left(\frac{\omega_x}{\omega_{xC}}\right)^2 + \left(\frac{\omega_y}{\omega_{yC}}\right)^2 + \left(\frac{\omega_z}{\omega_{zC}}\right)^2}$$

$$\text{with: } \omega_{xC} = 66.25 \frac{rad}{s}; \omega_{yC} = 56.45 \frac{rad}{s}; \omega_{zC} = 42.87 \frac{rad}{s}$$

$$P(AIS3+) = 1 - e^{-\left(\frac{BrIC}{0.987}\right)^{2.84}}$$



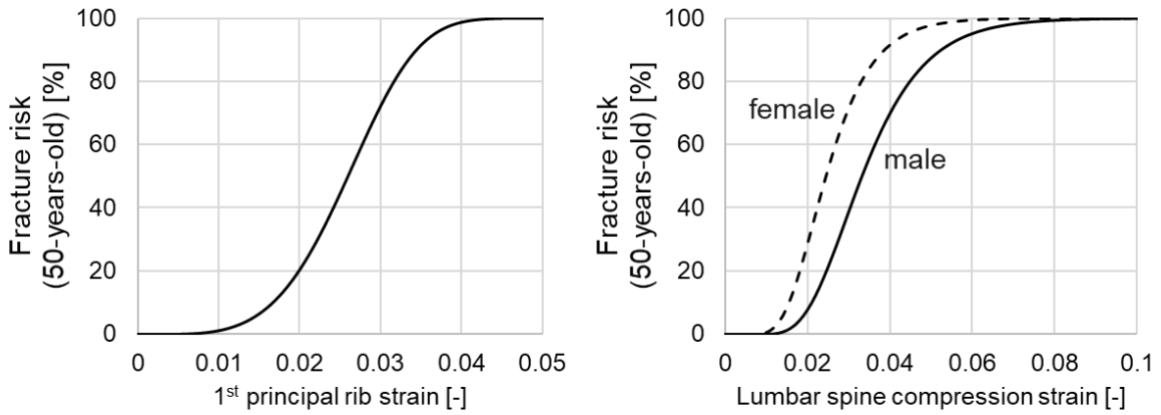


Figure 20: Rib (left) (Iraeus & Lindquist, 2021) and lumbar spine (right) (T5.2) fracture risk curves for a 50-years-old

The related functions are listed below (including the parameter values as stated in the corresponding reference):

Rib fracture (Iraeus & Lindquist, 2021) and number of fractured ribs (Forman et al., 2012):

$$\text{Fracture risk } (\varepsilon) = p_i = 1 - e^{-\left(\frac{\varepsilon}{\lambda}\right)^k}$$

with: $\lambda = 0.03658 * 0.0001655 * \text{Age}$; $k = 4.24954$; $\text{Age} = 50$

$$\text{Risk for exactly } X \text{ rib fractures: } \Pr(X) = \sum_{i=1}^{\binom{N}{X}} \left(\prod_{j \in C_i} p_j \right) \left(\prod_{k \in C_i} (1 - p_k) \right)$$

$$\text{Risk for } Y \text{ or more fractured ribs: } P_{\geq}(Y) = 1 - \sum_{X=1}^{(Y-1)} \Pr(X); P_{\geq}(3) = \text{NFR3+} = P(\text{AIS3+})$$

Lumbar spine fracture risk (developed in T5.2/Chalmers, described in D5.4):

$$\text{Fracture risk } (\varepsilon) = \frac{1}{2} + \frac{1}{2} \text{ERF} \left(\frac{\ln(\varepsilon) - (\beta_1 + \text{Age} * \text{coef}_{\text{age}} + \text{sex} * \text{coef}_{\text{sex}})}{\sqrt{2 * (\text{EXP}(\beta_2))^2}} \right) := P(\text{AIS3+})$$

with:

$$\text{coef}_{\text{sex}} = 0.3045; \text{coef}_{\text{age}} = -0.0118; \beta_2 = -1.0314; \beta_1 = -3.1178$$

ERF = Error or Gauss error function; EXP = Exponential function

Age = 50

$$\text{Sex} = \begin{cases} 0; \text{female} \\ 1; \text{male} \end{cases}$$



As input for the safety benefit assessment the following probabilities (P) will be calculated:

- P(AIS3+) skull fracture injury
- P(AIS3+) rotational brain injury
- P(lumbar spine fracture) = P(AIS3+) lumbar spine injury
- P(NFR3+) = P(AIS3+) thorax injury.

2.4 Estimation of the safety benefit

Having the results of the occupant simulations in Section 2.2 and the injury risk models per body region from Section 2.3, we can estimate the reduction of injured occupants as a result of an added-function car restraint systems. As stated earlier in Section 1, this report presents the methodology, the results of applying the methodology are going to be reported in T5.4.

The occupant injury reduction, for the specified crash scenario, is calculated by applying the dose-response method (Korner, 1989; Kullgren, 2008) in the following way (see also example in Figure 21).

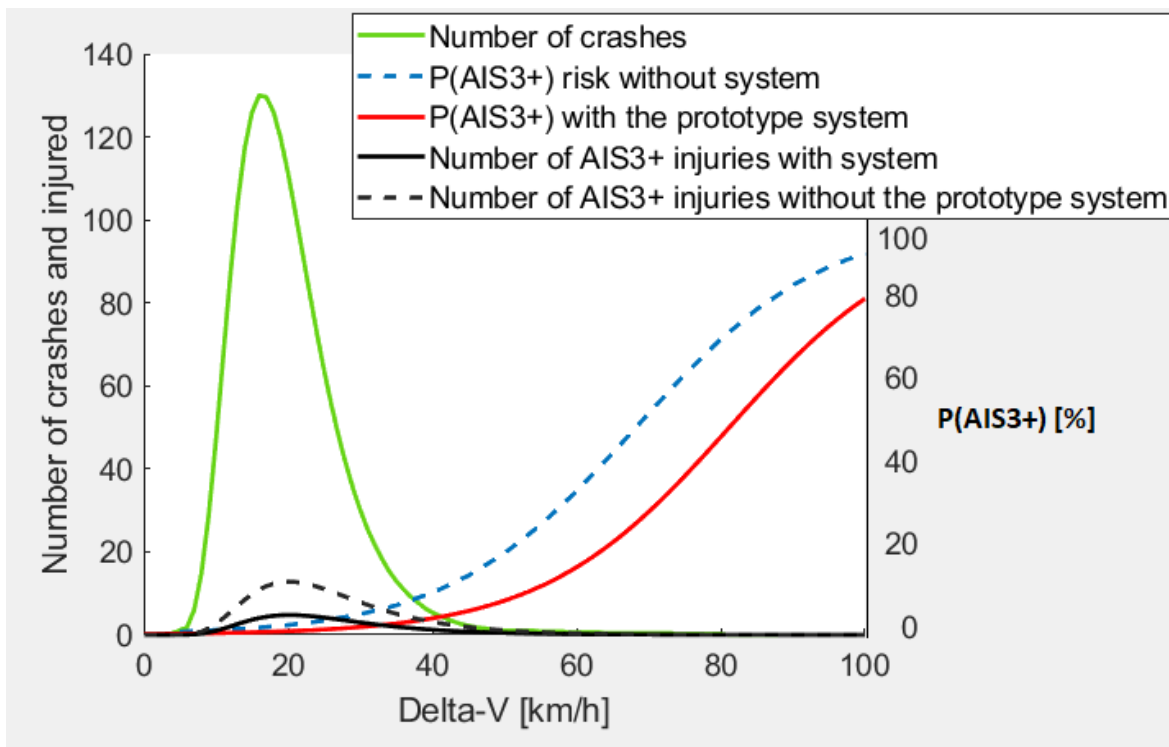


Figure 21: Dose response method exemplified for one system and one scenario.

For each body region, i , the overall injury probability $P_{BR_i}(I)$ per body region, is the integral of the product of ‘injury risk’ and ‘exposure’ conditioned on crash severity and integrated over the whole range of crash severities, in this case Δv , denoted as v :

$$P_{BR_i}(I) = \int_0^L P_{BR_i}(I|v) * s(v)dv \quad (1)$$



where L is the largest value v in the crashes, $s(v)$ is the probability density function of crash severity regardless of the injury outcome, and $P_{BR_i}(I|v)$ is the injury risk of a body region i given crash severity, v .

For the probability of the injury risk in terms of AIS3+ per body region, one injury criteria, from the ones specified in Sections 2.3, should be selected. For example, for body region 'head' the probability of AIS3+ injuries, the injury criterion 'BrIC' is used. As mentioned above, for the estimation of the safety benefit, all injury criteria need to be expressed using the same injury severity, e.g., AIS3+. To estimate the $P_{BR_i}(I|v)$ over the whole range of v , the following steps are done. First, we fit a linear function to BrIC as a function of v . In addition to any tested v values (ideally more than one), we will use (0,0) as another point. Using this function, we calculate the probability (p) of AIS3+ for the measured BrIC at the measured v using the BrIC function described earlier in Section 2.3.

For each body region i , the overall injury is expressed as $P_{BR_i}(I)$ for the baseline (state-of-the-art-system), while for the AF system, it is expressed as $P_{newBR_i}(I)$:

$$P_{newBR_i}(I) = \int_0^L P_{newBR_i}(I|v) * s(v)dv \quad (2)$$

Once the injury risk is calculated per body region, the overall injury risk (probability of any injury for the measured body regions), assuming that the injuries in the body region BR_i are independent, is estimated for the state-of-the-art system:

$$P_{Combined}(I) = 1 - \prod_i (1 - P_{BR_i}(I)) \quad (3)$$

and for the AF system

$$P_{newCombined}(I) = 1 - \prod_i (1 - P_{newBR_i}(I)). \quad (4)$$

The safety benefit in terms of relative reduction of occupant injuries by the improved system over the state-of-the-art system is calculated as

$$n = P_{Combined}(I) - P_{newCombined}(I). \quad (5)$$

The overall effectiveness, E , of the AF systems is the relative difference between the overall injury risk for the state-of-the-art system and the overall risk for the AF system:

$$E = \frac{P_{Combined}(I) - P_{newCombined}(I)}{P_{Combined}(I)} = \left(1 - \frac{P_{newCombined}(I)}{P_{Combined}(I)}\right) \cdot 100\%. \quad (6)$$

In the assessment, additional considerations need to be taken into account since the injury assessment criteria are not available for all body regions for the updated human body model. There might be multiple reasons for this. However, two reasons are identified here: some injuries are not measured in the HBM simulations, and some are measured but there is no injury risk function available at the time to estimate the probability of sustaining an AIS3+ injury. To take into account those other injuries that are not measured or not considered, we introduce a parameter X in the equations (3) and (4), which are updated as:

$$P_{Combined}(I) = 1 - \prod_i (1 - P_{BR_i}(I)) + X \quad (7)$$



$$P_{newCombined}(I) = 1 - \prod_i (1 - P_{newBR_i}(I)) + X_{new} \quad (8)$$

Using the occupant injury distribution from the in-depth data, X is calculated, and it is assumed that X is the same for the state-of-the-art system and the new AF system i.e., $X = X_{new}$. For example, X can be 0.2, if the rest of the other injuries from the original crash data are 20%. In the original data, there are more injuries than the injuries of the N body regions measured in the HBM simulations (e.g., in the original data, there are other injuries than the head, thorax and lumbar injuries). There are also other injuries, such as neck injuries that are measured in the HBM simulations, but do not have a corresponding transformation by the IRF to AIS3+. They can therefore not be included in the model in the equation eq. (3) and (4), but they are to some extent counted in the parameter X .

The following possible assumptions can be considered depending on the observed crash data and the results from HBM simulations. First, assumption A1 is that X is the same in the SOTA and the AF system, i.e., $X = X_{new}$. Second, assumption A2 is that X is not the same for the SOTA and the AF system, i.e., $X \neq X_{new}$. Assumption A1 embodies the notion that the AF system has no effect on any body region that wasn't tested in simulation. Assumption A2 contains all other possibilities.

One possibility for assumption A2 is that those body regions that could be observed in simulation are representative of all body regions, and thus percent in improvements to those body regions will be reflected in percent improvements for all body regions. In that case $X_{new} = X * E$. Alternatively, there can be some improvements in unmeasured body regions, but they may be less than for the tested body regions. Since there is no direct information about untested body regions, a reasonable range of the values of X and X_{new} can be considered and a sensitivity analysis for that range can be performed when calculating and reporting the benefit.

In the original data, the number of observed injuries should be higher than in our models (because there are also other injuries in the original data that are not taken into consideration in the models, and the HBM simulations are performed with one or few values of v , for example, VIVA+ HBM model). If the number of injuries from the HBM simulations and the applied models are larger than in the original data, then 'scaling up or down' should be performed. This type of 'scaling' will use the injury distribution of Max AIS0-6 injuries.

The overall effectiveness E is estimated for the following cases included in the simulation matrix (see Table 7):

- 'Upright (nominal) seating position with SOTA restraint type without AEB system' vs 'Lean forward seating position with SOTA restraint type with AEB'.
- 'Lean forward seating position with SOTA restraint type with AEB' vs 'Lean forward seating position with AF restraint type with AEB'.
- 'Reclined with lean forward seating position with SOTA and AEB' vs 'Reclined with lean forward seating position with AF restraint system and AEB'.



In the cases where SOTA systems are compared with the AF systems and an AEB system is present, a generic AEB will be applied. That is, separately, the v distribution for a specific crash scenario where AEB would work is shifted far enough to put a target percentage of crashes below a v of 0 (i.e., prevented or v is shifted to the left by 10kph (Volvo Cars, 2022)). For new oncoming AEB safety systems for oncoming vehicles, this shift is done according to recent 'owners manuals' and consumer testing procedures (Euro NCAP, 2022a; EURO NCAP, 2021; Volvo Cars, 2022). (There is no literature study of the effectiveness of AEB for oncoming vehicles. Therefore, the above assumption about the shift of the v distribution is considered. When such AEB systems for oncoming vehicles are released to the market, the same procedure can be applied with updated values for the AEB effectiveness.)

When the AEB-based reduction is applied, followed by the v distribution details (explained above) of the safety system, it can be estimated how many crashes will be avoided plus how much injury risk reduction occurs by having the AF restraint systems.

2.5 Market penetration

Having the weighted v distribution allows to directly obtain the safety benefit results, i.e., reduction of occupant injuries in EU in a corresponding year (e.g., 2018) if all cars are equipped with the new passive safety system, assuming a market penetration rate of 100%. The system performance and expected results are computed as described above. These results assume a fleet penetration rate of the system of 100%. In general, especially the fleet penetration of 100%, is not reached instantly but over a rather long period.

In this assessment, for reasons of simplicity, it shall be assumed that a market penetration of a given percentage (x%) also results in the corresponding number of reduced casualties compared to the maximum benefit (e.g., only x% percent of casualties are "really" prevented by the system).

The safety benefit can be calculated based on the avoided injuries (system performance) in consideration of a market penetration for the respective year, using the following formula:

$$SB_{year,injury} = (n_{injury}) * mp_{year}$$

where SB refers to the safety benefit, n to the number of avoided casualties per injury severity (AIS3+) from (5), assuming a market penetration of 100%, and mp refers to the market penetration in the respective year.



3. Demo 2

Demo 2 focusses on the assessment of exemplary Radar, LIDAR, and camera performance in adverse weather conditions. The performance itself is assessed in terms of visibility of pedestrians, PTWs and, bicyclists in different rain rates and fog densities, see also D3.5. As a result of this assessment, a “weather filter” has been developed, which can be deployed on an ideal object lists (ground truth object information) to mimic weather effects in terms of reduced visibility range in simulation. Additionally, a FOV radar and camera sensor has been developed, which also is available for simulation. The weather filter by itself is not representing a technology which can reduce KSI by deployment in vehicles, but this filter supports the analysis of sensors and their different sensitivity to rain and fog. Thus, it enables a hypothetical safety performance assessment of advanced sensor and perception systems, in bad-weather situations via simulation.

In D2.6, use-cases have been identified which are specifically relevant for adverse weather conditions, those shall be used as baseline for the performance assessment. For pedestrian scenarios, two main use-cases were found for which precipitation leads to more accidents than normal weather conditions. These are the use-cases P-CLwoSO (Pedestrian crossing left without sight obstruction) and P-PCTurnL (Passenger car turning left). For the bicyclist, use-cases B-CR (Cyclist crossing from right while PC moves forward) and B-PCTurnL (Cyclist in conflict with PC turning left) are selected for special consideration in precipitation. The GIDAS-PCM cases are modified as described in Section 1.2.1.1.

With this background, a modification to the initial research question defined in D5.1 (Mensa et al., 2021) shall be answered:

“What is the hypothetical safety performance of an active safety system with an ‘all-weather VRU detection system’ at a penetration rate of 100% in Car to VRU collisions on urban roads in terms of KSI injury reduction on EU level in 2025 compared to the 2016 numbers and the same safety system with SOTA VRU detection system?”

The newly developed weather filter will be used to assess the effect of advances of increased visibility in sensor technologies in adverse weather conditions. Since current simulation processes and toolchains often neglect weather effects on sensors this will help to understand these situations better. The following section elaborates the “all weather VRU detection system” and the “SOTA VRU detection system” further.

3.1 Simulations

This section describes the simulations to be performed for Demo 2. The baseline technology is a SOTA AEB and VRU detection system – deployed as camera and radar FOV-models, with ranges dependent on the weather situation and with an ideal perception, which means as soon as the object enters the FOV, it is classified. The active safety system is defined as an SOTA AEB with a TTC based triggering, see section 1.2.1.3. The “all weather VRU



detection system” (treatment) technology is defined as an advanced sensor with less visibility reduction in bad weather situations. In this case it is assumed, that this sensor will have the same FOV in all weather conditions as in good weather conditions.

3.1.1 Baseline

ZF has developed a process to re-simulate GIDAS PCM cases in the IPG CarMaker simulation environment, see section 1.2.1. The corresponding PCM scenarios included in P-CLwoSO, P-PCTurnL, B-Cr and B-PCTurnL will be assessed with a baseline weather filter model and a treatment model which shall represent a higher fidelity model for adverse weather.

3.1.2 Simulation models

To assess the weather effect in terms of accident avoidance, the weather effects are transferred into a simulation environment. The challenge is the multitude of possible weather conditions and their individual influence on each sensor. For this purpose, the measurement campaigns mentioned in Deliverables 3.2 (Löffler & Gloger, 2021) and 3.5 (Löffler, Vogl, et al., 2022) were conducted to investigate the influence of weather conditions on perception. The partly static and partly dynamic measurements are used to investigate the maximum detection distance of the VRU object class to the sensors. The detection of VRUs depends on the reference angle to define the FOV and reconstruct selected crash scenarios with subsequent evaluation from the point of view of the perception unit up to the impact location. Since not all possible weather scenarios can be tested, the weather filter from Deliverable 3.5 (Löffler, Vogl, et al., 2022) is developed as a simulation model for the sensor classes LIDAR, camera and radar, where the measured values from the measurement campaigns serve as reference values and are used accordingly for arbitrary weather conditions in the range of 0-100 mm/h (rain) and 5-10,000 meters visibility (fog). As described in Deliverable 3.2 (Löffler & Gloger, 2021), real-world tests are subject to the limitations of the CARISSMA test facility. Due to the limitation of the rain measurements to a total area of 4x50 m is also virtually augmented and extended with the weather filter and the FOV filter.

3.1.2.1 Vehicle model and VRU model

For the simulations from ZF, the CarMaker tool has been used and a high-fidelity vehicle dynamics model of a Toyota RAV4 was chosen, since this was the correlating vehicle used for physical testing of Demo 4. Due to simplification of the simulation process the same model is applied for Demo 2 assessment. The pedestrian model represents a typical male adult character with a running and walking motion animation. The cyclist-model represents a female city-bike cyclist. The respective dimensions are described in





Figure 22: IPG CarMaker visualization of VRU and vehicle model vehicle architecture idealization approach 2.

Table 9: Dimensions of CM-models.

Class	Dimension Length x Width x Height
Pedestrian	0.34m x 0.60m x 1.80m
Cyclist	1.80m x 0.70m x 1.75m
Car (Rav4 2019)	4.60m x 2.26m x 1.72m

3.1.2.2 Sensor and Perception model

The sensor system used for simulation is the weather filter created by Cariad and documented in D3.5. The baseline FOV-model will have different FOV settings in adverse weather conditions according to the given rain rates. The treatment weather filter is modelled to not be influenced by any weather condition.

Figure 23 shows the resulting FOV for a pedestrian target which is orientated perpendicular to the sensor, this model will be used as a sensor model for the simulation. The used GIDAS-PCM scenarios have a variety of pedestrian and cyclist orientations. A radar and camera FOV investigation has not been performed for cyclists.



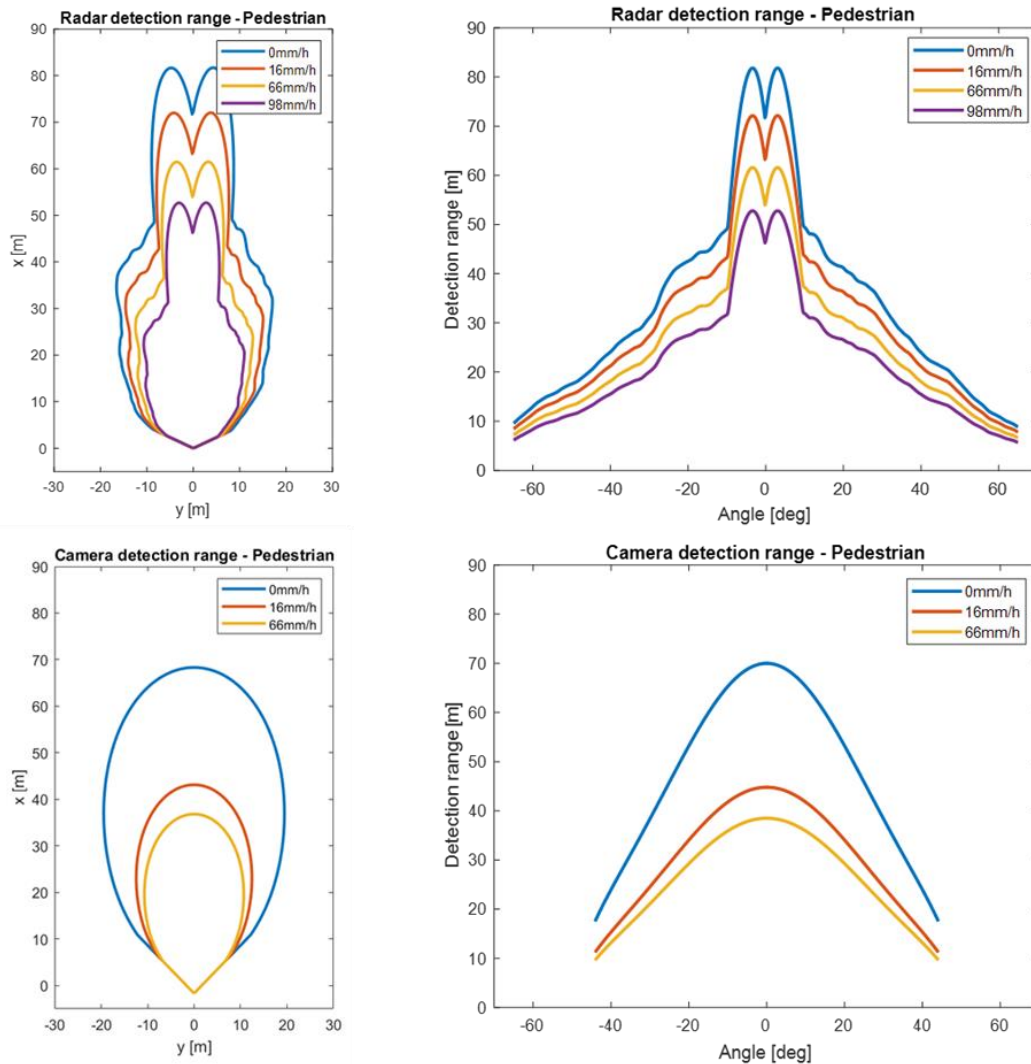


Figure 23: FOV of investigated radar (top) and camera (bottom) sensor at dry and rainy conditions in Cartesian coordinates (left) and polar coordinates (right), taken from D3.5, figure 23.

An analysis of different pedestrian and cyclist target orientations shows that a pedestrian perpendicular to the sensor provides the lowest visibility range for cyclist and pedestrian targets in various orientations (see Figure 24 and Figure 25). Using this FOV-model not respecting the orientation of the target in the simulation will provide worst case results.



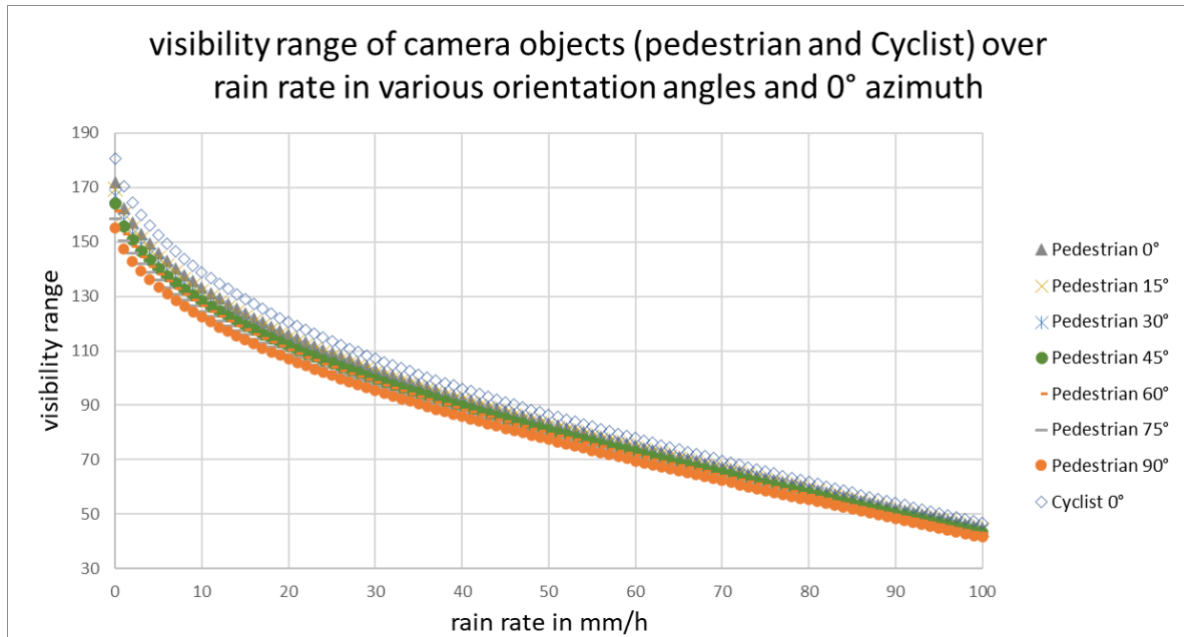


Figure 24: Camera object visibility in over rain rates in various orientations to the sensor at 0° azimuth.

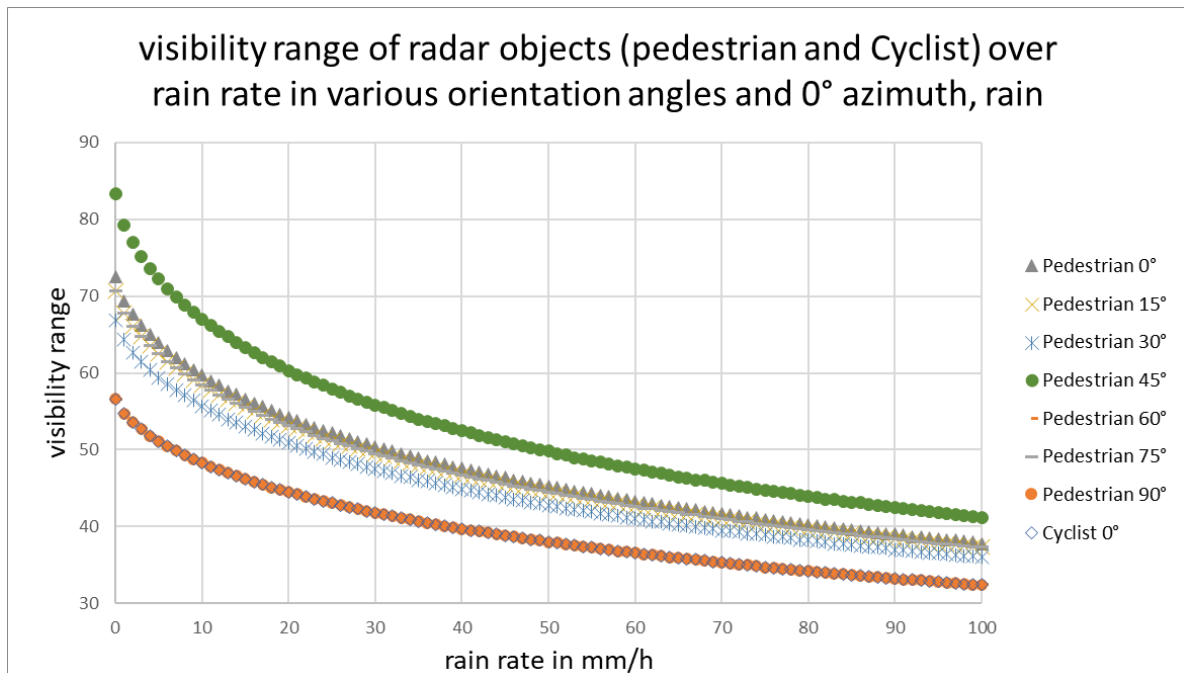


Figure 25: Radar object visibility in over rain rates in various orientations to the sensor at 0° azimuth.



4. Demo 3

In Demo 3, advanced vehicle dynamics intervention functions are developed to avoid or mitigate critical events. The demonstration vehicle includes an algorithm capable of combining both emergency braking and steering.

For the emergency steering functionality, electronic power steering as well as differential braking are investigated regarding their accident-avoidance potential in the defined scenarios.

In case of emergency, advanced intervention functions will be triggered to avoid critical events, including naturalistic crash mitigation manoeuvres, enhanced emergency functions for crash avoidance (AES, AEB), and minimisation of the sidestep distance.

Further details on Demo 3 can be found in D3.1 (Nikolaou & Panou, 2021) and D3.3 (Löffler et al., 2021).

The Demo 3 assessment is conducted to answer the following research question:

“What is the safety performance of an ‘VRU AEB+S’ at a market penetration rate of 9.6% / 27.5% / 100% in car to VRU collisions on urban roads in terms of KSI reduction on EU level in 2025 compared to the 2016 numbers?”

To answer this research question, virtual simulations are conducted to compare a baseline (without system) to the treatment (with system), see Section 4.1. In those simulations, all involved components (Ego vehicle, VRU, sensors, the technology under test, etc.) are represented virtually. These simulations aim to represent the Demo 3 ‘VRU AEB+S’ system, which decides autonomously whether to conduct an emergency in-lane evasion manoeuvre or an emergency braking manoeuvre. Furthermore, the real system is tested physically in a defined set of scenarios, see Section 4.2.

4.1 Simulations

This section describes the implemented systems’ algorithms and the simulation tools used for the virtual simulations.

In the baseline, it is assumed that no collision mitigation system is installed. For the treatment simulations, the VuT is equipped with the VRU AEB+S system. The baseline is compared to the treatment on a case-by-case basis to compute the avoidance rate.

4.1.1 Baseline

To generate the baseline for Demo 3, the approach described in Section 1.2.2 is applied. The resulting ranges for the initial velocity of the VRU and VuT are shown in Table 10 and Table 11. Due to the technical calibration of the simulated AEB+S system, we restrict the



initial velocity such that $v_0 \in [v_{min}, v_{max}]$, yielding the remaining scenarios provided in Table 10 and Table 11.

Table 10: Ranges for the initial velocity to be simulated for each individual car-to-pedestrian use-case (C2P).

Use-case	VuT range in kph	Coverage of cases within use-case	Coverage of total cases	VRU range in kph	Coverage of cases within use-case	Coverage of total C2P cases
CRwoSO	30-60	71.9%	16.7%	2-10	96.4%	22.4%
CRwSO	30-55	63.1%	11.9%	2-10	98.9%	18.6%
CLwoSO	30-60	85.9%	16.7%	2-10	99.1%	19.3%
CLwSO	30-50	59.7%	8.3%	2-6	94.1%	13.2%

Table 11: Ranges for the initial velocity to be simulated for each individual car-to-bicycle use-case (C2B).

Use-case	VuT range in kph	Coverage of cases within use-case	Coverage of total cases	VRU range in kph	Coverage of cases within use-case	Coverage of total C2B cases
CRwoSO	30-50	36.9%	5.6%	4-26	95.7%	14.5%
CRwSO	30-50	36.9%	8.3%	4-26	96.2%	21.8%
CLwoSO	30-50	31.5%	2.6%	4-20	84.5%	6.9%
CLwSO	30-35	6.6%	1.1%	4-26	91.6%	15.8%

In addition to the initial velocity for the VuT and VRU, also the lateral impact location factor on the VuT (p_{VRU}^{lat} , see section 1.3.1) is varied between -0.05 and 1.05 (C2P use-cases) and -0.45 and 1.45 (C2B use-cases). The location of the sight obstruction (if present) is varied with $D_l - 0.5m$, D_l , $D_l + 0.5m$ (see Figure 14), where D_l is the original value from the Euro NCAP protocol. The lane width w_{lane} is varied between 3.0m and 3.75m. The lateral position factor of the VuT on the lane (p_{VuT}^{lat} , see section 1.3.1) is varied between 0.4 and 0.6.

4.1.2 Simulation models

To perform the simulations for safety performance assessment, several models need to be combined. This is done using a co-simulation approach with the software Model.Connect as a co-simulation platform. The basic set-up of the co-simulation is shown in Figure 26. The models to be coupled are:

- driving dynamics of the VuT,
- traffic around the VuT,



- infrastructure around the VuT,
- driver of the VuT,
- sensor,
- algorithms of the safety system.

The respective models will be described in 4.1.2. The coupling itself and the simulation management is done via Model.Connect. Model.Connect covers the whole simulation process, i.e., it starts the respective simulation tools, manages the dynamic data exchange between the coupled models, stores the results and closes the simulation tools at the end of each simulation run. Moreover, Model.Connect can start a set of simulation runs either in sequential or parallel way. This feature is used to perform the simulation of all baseline and treatment cases in one batch.

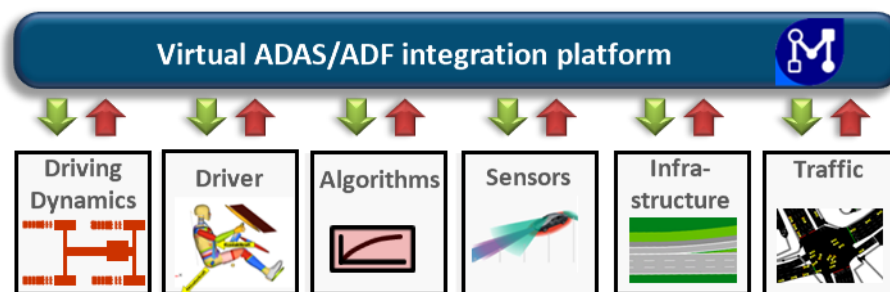


Figure 26: Schematic of the co-simulation set-up.

The individual models to be coupled are described in the following subsections.

4.1.2.1 VuT Driving dynamics model

In the Demo 3 simulations, driving dynamics of the VuT are represented by a “Single-Track Drift” (STD) model. A description of this model can be found in Althoff & Würsching (2020). The STD model extends the well-known bicycle or “Single-Track” (ST) model, which is described, for example, in Rajamani (2012), Section 2.3. In the ST model, vehicle dynamics are simplified by small angle approximations and linear tire dynamics. However, the AES system in Demo 3 introduces highly dynamic manoeuvres, which is why using the STD model is required, introducing the following additions compared to the ST model:

- No small angle approximations for the steering and slip angles are used;
- Longitudinal tire forces and longitudinal slip are modelled for the rear and front wheels individually;
- The Pacejka tire model (Pacejka, 2012) is applied to compute the tire forces, considering combined slip.

The geometrical parameters in the STD were adapted to fit the real vehicle used in the physical tests for Demo 3 (see Section 4.2). For collision detection, the geometry shown in Figure 27 was used, which corresponds to the contour line of the real vehicle (as seen from



bird's eye view without the side mirrors) used in the physical tests. Using measurements from the physical tests, a validation of further model parameters was conducted.

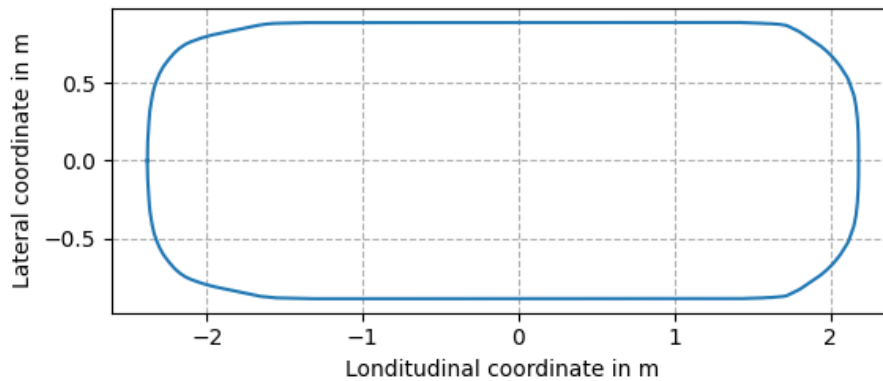


Figure 27: Vehicle geometry used for collision detection. The vehicle front is on the right side of the Figure.

4.1.2.2 Traffic model

The traffic around the VuT is represented by the VRU, which in turn is represented by a simple point-mass-model with a pre-defined velocity profile and trajectory. For collision detection, the geometries for the pedestrian and cyclist targets (EPTa and EBT) defined in the EuroNCAP protocol (Euro NCAP, 2022b) are used, see Figure 28.

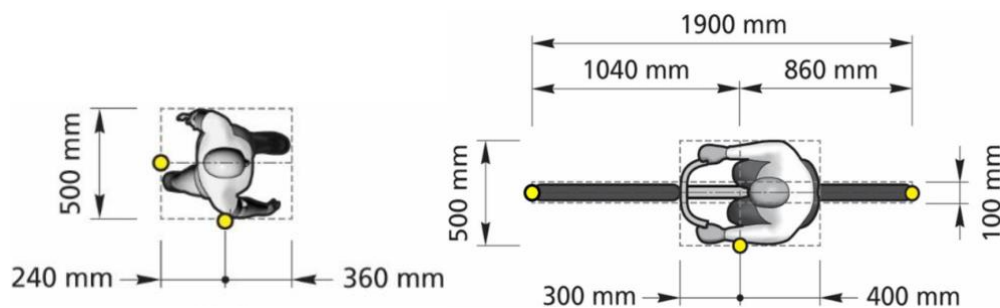


Figure 28: VRU geometries EPTa (left) and EBT (right) (Euro NCAP, 2022b).

4.1.2.3 Infrastructure model

This part of the simulation represents the relevant static elements. These are:

- The road on which the VuT drives along including road- and lane-markings. The lane markings are relevant for defining the space available for lateral avoidance as the technology under assessment is designed so that VuT must stay within the current lane during the evasive manoeuvre. The road information is stored in the OpenDRIVE (*.xodr) format.
- Obstacles obstructing sight. These might delay the point in time where the VRU becomes visible, making a situation more critical than without visual obstruction.



4.1.2.4 VuT Driver model

As driver reactions to the scenario are not considered in this study, a trajectory following driver model is used. The driver model features used in this study are limited to controlling the longitudinal dynamics, i.e., the speed of the VuT. For that purpose, a PID controller is used. In principle, the applied driver model is also capable of performing lateral control. As the lateral control will be performed by the safety technology under assessment for the simulated time range, this feature is not used in this study.

4.1.2.5 Sensor model

In the simulations, a simple geometrical sensor model was used. The sensor is located at the middle of the vehicle front. The sensor field of view can be represented by a circle sector, with the radius corresponding to the range of the sensor, see Figure 29. For the simulations for Demo 3, the radius was chosen to be 150m and the opening angle 100°, based on the sensor that was used in physical testing.

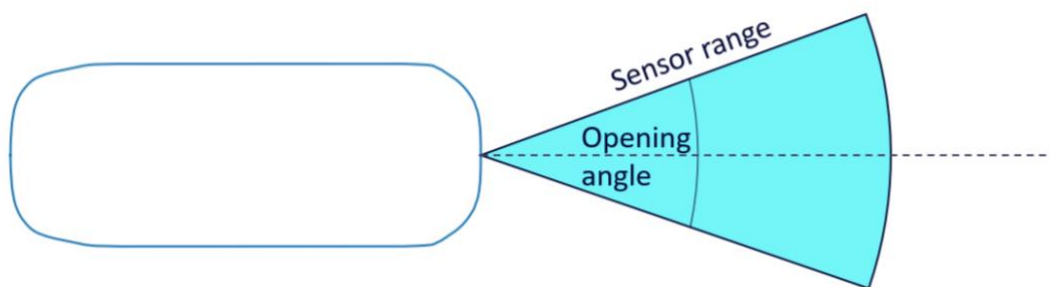


Figure 29: Schematic representation of the sensor field of view.

4.1.2.6 System model

The actual Demo 3 software is integrated into the simulation framework as the Demo 3 system model. It consists of several functionalities developed by different partners. Figure 30 shows the high-level interactions between the functionalities developed by the partners for Demo 3. These functionalities are implemented in the ROS2 (Robot Operating System) framework, which acts as a middleware and facilitates communication between the functionalities. The ROS framework also provides the communication interface to the full simulation framework (Section 4.1.2). Within the ROS framework, the functionalities are implemented as separate executables (nodes), and these nodes communicate with each other via broadcast messaging, using a publisher-subscriber pattern (Löffler, Gloger, et al., 2022).



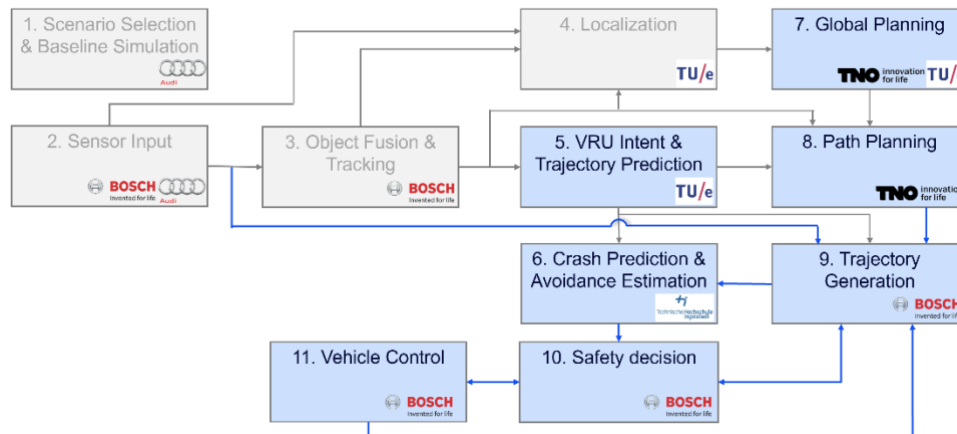


Figure 30: High level interaction layouts between Demo 3 functionalities. Subsystems relevant for the simulations are marked in light blue (Löffler, Gloger, et al., 2022).

Subsystems relevant for the simulations are marked in light blue. Subsystems marked in white are replaced by the simulation framework. The arrows between the blocks indicate the information flow. In this Figure 30, the main flow from sensor input to controller output is from left to right.

The VRU intent & trajectory prediction (5) predicts the intent and trajectory of VRUs. The path planner (8) plans a path and a global route, provided by the global planning (7). This global planning needs the current location of the vehicle, provided by the localization (4) module. The trajectory generator (9) generates trajectories based on the planned path and the predicted VRU trajectories. The trajectories are evaluated on their risk for a collision, which is provided by the crash prediction and avoidance function (6). The selection and handling of planned trajectories is performed by the Safety decision (10) module. Finally, the vehicle control (11) generates the outputs to control the vehicle to follow the generated trajectory.

Specifically, for the WP5 simulations, input and output wrappers converting the signals into the needed format for the ROS framework are implemented. Figure 31 contains an overview of the interfaces between the Virtual Vehicle Model.CONNECT framework and the Demo 3 ROS2 framework.



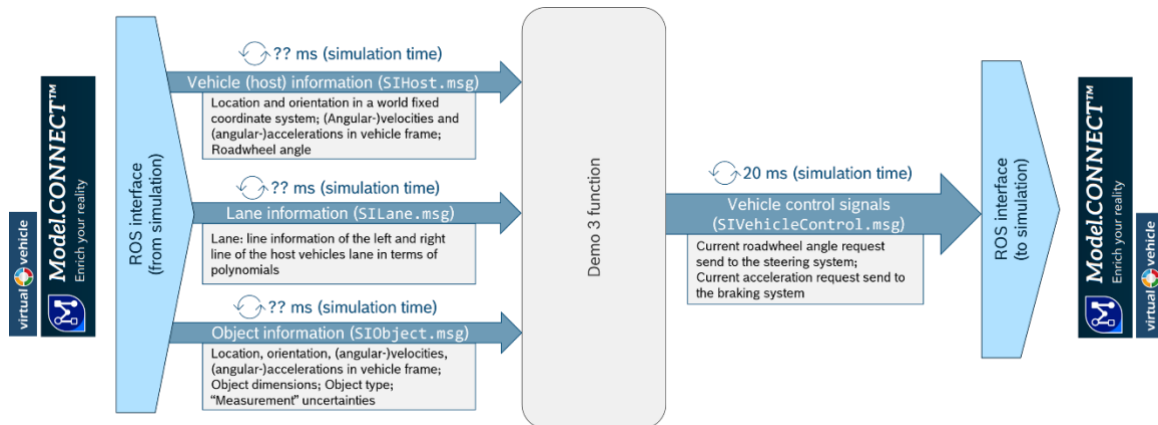


Figure 31: Interfaces between the Virtual Vehicle ModelCONNECT framework and the Demo 3 ROS2 framework.

An extensive description of the Demo 3 subsystems can be found in the deliverable D3.6 (Löffler, Gloger, et al., 2022).

4.2 Physical testing

The physical testing of Demo 3 was performed during 4 days at the IDIADA proving ground facilities in Santa Oliva, Spain, using the BOSCH Demo 3 vehicle as well as state-of-the-art VRU dummy test systems. The general purpose of the test campaign was the generation of the accident avoidance rate statistics needed for the safety benefit assessment to provide real world evidence to the simulation results for a low number of test scenarios but with a rather high number of repetitions per scenario. These repetitions per scenario are needed due to the scattering VRU detection performance, leading to different trigger timing for the avoidance system and hence to different accident avoidance outcomes. Figure 32 shows an impression from the test campaign.



Figure 32: Impression from Demo 3 physical testing.



The following scenarios were tested using both AES and AEB, with approximately 10 runs per system setting (AEB or AES):

- **P-CRwoSO**, frontal, close corner, ego vehicle speed $v_{Ego} = 50$ kph, pedestrian speed $v_{Ped} = 6$ kph, lat. impact location = 0% (Pedestrian crossing from right, leading to a frontal impact on the right edge of the vehicle's front)
- **P-CRwoSO**, side, ego vehicle speed $v_{Ego} = 50$ kph, pedestrian speed $v_{Ped} = 6$ kph, long. impact location = 30% (Pedestrian crossing from right, leading to a side impact on the first third of the vehicle's side).
- **P-CRwSO**, frontal, close corner, ego vehicle speed $v_{Ego} = 50$ kph, pedestrian speed $v_{Ped} = 6$ kph, lat. impact location = 0% (Pedestrian crossing from right, leading to a frontal impact on the right edge of the vehicle's front)
- **P-CRwSO**, side, ego vehicle speed $v_{Ego} = 50$ kph, pedestrian speed $v_{Ped} = 6$ kph, long. impact location = 30% (Pedestrian crossing from right, leading to a side impact on the first third of the vehicle's side).

To generate the late object detection that makes the AES necessary for a complete avoidance manoeuvre, all of the scenario parameter combinations for the cases with sight obstruction were tested with different obstruction settings, where the obstruction was placed in such a way that 1m, 1.5m and 2m of lateral distance between the obstruction and the outer edge of the vehicle's lane remained.

Both pedestrian speed and impact location parameters were not varied during the test campaign, as the performance was satisfying even with the worst-case parametrization as described above. As the changes mainly result in a change in detection timing, their effect is expected to be estimated in post-processing as well.

A detailed description of the selected Demo 3 scenarios can be found in the deliverable report D3.6 (Löffler, Gloger, et al., 2022).



5. Demo 4

The Demo 4 aimed to answer three research questions (RQs), which were initially presented in D3.4, (Nikolaou et al., 2021) and are summarised below:

RQ 1: “What is the safety benefit of a VRU C-ITS warning system on connected VRUs in supporting them to mitigate safety-critical events with passenger cars, triggered by a radio signal based (OBU, VRU-smart device) communication and detection system, in terms of KSI injury reduction on EU level in 2025 compared to the 2016 numbers for Car to VRU collisions on urban roads?”

RQ 2: “What is the safety benefit of a VRU C-ITS warning system on vehicle drivers in supporting them to mitigate safety-critical events with connected and non-connected VRUs, triggered by a radio signal based (OBU, RSU, VRU-smart device) communication and detection system, in terms of KSI injury reduction on EU level in 2025 compared to the 2016 numbers for Car to VRU collisions on urban roads?”

RQ 3: “What is the safety benefit of a vehicle equipped with an active safety system (e.g., AEB) that is enhanced by a radio signal based (OBU, RSU, VRU-smart device) communication and detection system, in terms of KSI injury reduction in EU urban roads in 2025 compared to the 2016 numbers and the same safety system with SOTA VRU detection system?”

To answer each of the questions, Demo 4 develops a VRU safety system based on V2X technology that provides enhanced communication between vehicles, road infrastructure (RSU installed nearby) and VRUs (pedestrians and cyclists). The actual target is to provide additional environmental perception to vehicles regarding the presence of VRUs in critical situations, especially in cases where the vehicle sensors reach their limits (i.e., obstructed areas). Connected VRUs are able to directly exchange V2X messages with the equipped V2X vehicles, whereas the non-connected VRUs are monitored by the RSU that exchanges messages with the V2X equipped vehicles.

The vehicle is equipped with an AEB system based on perception sensors that may be engaged in cases where an immediate emergency stop is required. This AEB system will potentially increase its efficiency in certain scenarios in combination with V2X technology. Data from perception sensors and V2X information will feed the AEB system in order to be engaged on-time and to perform an earlier system reaction in situations with limited sensor perceptibility. With high V2X localization accuracy, the system reaction could have the potential of an earlier AEB intervention. More details of the Demo 4 are available in D3.4 (Nikolaou et al., 2022).

RQ1 focusses on the assessment of the mitigation of a safety critical event, based on the warning and the reaction to that warning from the viewpoint of an VRU. A V2X-based warning function on bicyclists has been developed, which will be assessed to the Baseline GIDAS-PCM data which is available for cyclists. A TTC-based warning-trigger model and a time-to-stop over cyclist velocity model for the bicyclist will be created based on the



experiments of Demo 4. This will be applied on the cyclist PCM-trajectories to evaluate the ability of a warning in mitigation of critical events. That means that the treatment simulations are performed with VRU warning when the cyclists are connected (V2X connectivity); the cyclist responds to the warning with the typical cyclist reaction to stop (described above). The baseline for this assessment is the GIDAS-PCM data without modifications for Demo 4 (Approach A).

To answer RQ2 the same simulations as for RQ3 will be performed but the applied modification for the baseline is changed. No AEB-System will be deployed but a FCW-System with a driver model (with typical reaction times and deceleration curves), see Section 1.2.1.3. In the baseline simulations the VRUs are not-connected. The treatment simulations will be performed with connected VRUs, where a “treatment FCW” is deployed. The “treatment FCW trigger” timing will be obtained from the physical test performed for Demo 4. In both cases, baseline and treatment, driver model (with typical reaction times and deceleration curves) will be applied.

To answer RQ3 simulations and physical testing are performed which are described in Section 5.1 and 5.2, respectively.

5.1 Simulations

Simulations for the Demo 4 scenarios were realized by IDIADA and by ZF with different purposes. IDIADA has simulated all Demo 4 scenarios with the same parameters (e.g., speeds of the VUT and VRU) as the physical testing to validate the technical solution. ZF performs simulations to assess the safety performance of Demo 4, with baseline approach B. However, IDIADA’s simulations results may also be taken into account for the impact assessment. In this section, details from both simulations are available. These simulations are focusing on answering RQ3.

5.1.1 Baseline for simulations by IDIADA

The suggested velocity ranges for each use-case are shown in Table 12 and Table 13. For the method to define the velocity ranges, see section 1.2.2. From the suggested velocity ranges, IDIADA has simulated the use-cases and the velocity ranges shown in Table 14 and Table 15. Section provides technical details how the scenarios were setup in the simulation environments. In baseline, none of the actors (VuT and VRU) are connected via V2X. Only the AEB function from the VuT is active in order to extract a reference performance of such AEB which will be compared with the results of the AEB with V2X from the treatment.



Table 12: Ranges for the initial velocity to be simulated for each individual use-case (C2P).

Use-case	VuT range in kph	Coverage of cases within use-case	Coverage of total cases	VRU range in kph	Coverage of cases within use-case	Coverage of total cases
TurnL-SD	15-40	83.0%	7.7%	2-6	94.1%	8.8%
CRwSO	25-55	83.1%	15.6%	2-10	98.9%	18.6%
CLwSO	20-50	85.3%	11.9%	2-6	94.1%	13.2%

Table 13: Ranges for the initial velocity to be simulated for each individual use-case (C2B).

Use-case	VuT range in kph	Coverage of cases within use-case	Coverage of total cases	VRU range in kph	Coverage of cases within use-case	Coverage of total cases
TurnL-SD	15-40	81.8%	8.2%	4-20	85.7%	8.6%
CRwSO	5-50	91.9%	20.9%	4-26	96.2%	21.8%
CLwSO	5-35	82.4%	14.3%	4-26	91.6%	15.8%

Table 14: Ranges for the initial velocity simulated for each individual use-case (C2P) by IDIADA.

Use-case	VuT range in kph	Coverage of cases within use-case	Coverage of total cases	VRU range in kph	Coverage of cases within use-case	Coverage of total cases
TurnL-SD	10-30	69.7%	2.8%	5, 8	24.6%	1%
CRwSO	25-65	79.1%	13.3%	5, 8	32.7%	6%

Table 15: Ranges for the initial velocity simulated for each individual use-case (C2B) by IDIADA.

Use-case	VuT range in kph	Coverage of cases within use-case	Coverage of total cases	VRU range in kph	Coverage of cases within use-case	Coverage of total cases
TurnL-SD	10-30	62.4%	1%	15-20	41.4%	0.6%
CRwSO	15-30	30.4%	3.5%	15-20	47.9%	5.5%
CLwSO	15-30	40.9%	2.6%	20	14.3%	0.9%

5.1.2 Baseline for simulations by ZF

The Baseline definition for Demo 4 by ZF is described in 1.2.1.2.



5.1.3 Simulation models

5.1.3.1 System model

Virtual simulation of systems and technologies also means the development of a simulation model which represents the device under test appropriately. The simulation model is developed to fulfil the simulation requirements but do not represent the real developed technology. Demo 4 with its set up is complex and a reduction of complexity for simulation is needed. ZF decomposed the vehicle system and created an idealization of the system for the simulation as shown in Figure 33. It can be seen that the multiple sensors and the vehicle perception is idealised to an ideal perception (ground truth perception). Especially the added benefit of Road-Side-Units (RSU) and VRU-Communication devices shall enable a vehicle perception to get closer to an ideal perception unit.

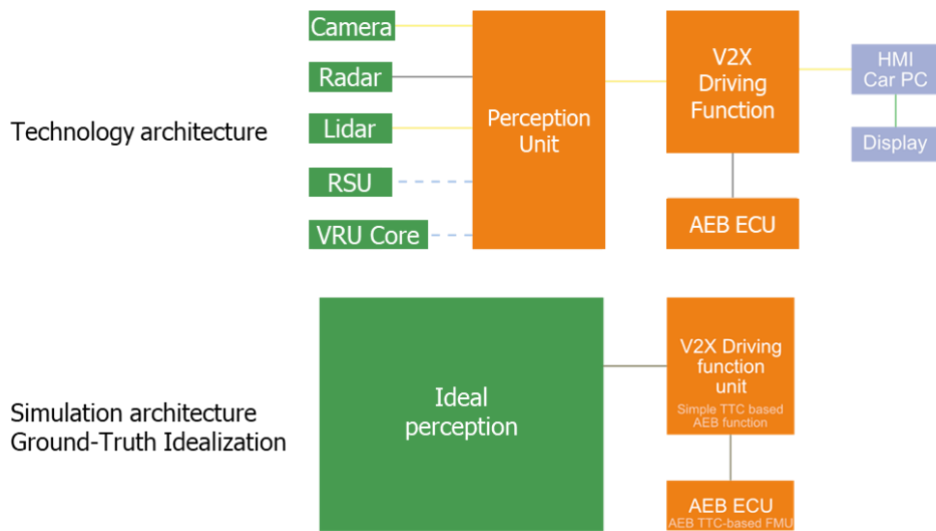


Figure 33: Vehicle technology architecture (from D3.9) in comparison to simulation architecture.

A more realistic idealization of the vehicle architecture is illustrated in Figure 34. This idealization enables the Perception Unit to distinguish between object data from the vehicle internal sensors and the objects from the RSUs. Thus, it is possible to assess also possible latency and signal flow effects for the assessment of the performance benefit of the RSU-System.



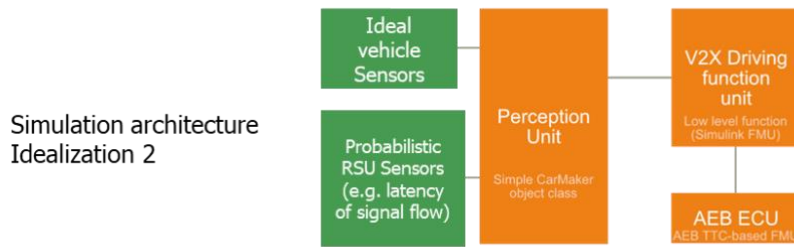


Figure 34: Demo 4 vehicle architecture idealization approach 2.

Additionally, to the idealization of the sensor and perception system, the function logic and AEB-ECU have to be modelled. Since the V2X-software unit and the AEB-ECU couldn't be shared, a model has been created which represents the real system as closely as possible, see also Section 1.2.1.3.

5.1.3.2 Vehicle model and VRU model

ZFs simulation are performed with IPG CarMaker. A detailed description of simulation models can be found in Section 3.1.2.1.

For IDIADA simulations, the VuT model consists of dSPACE's ASM Vehicle Dynamics model, which is based in a nonlinear multibody vehicle system that supports the simulation of vertical, longitudinal, and lateral dynamics.

It is important to note that the model contains the vehicle and an environment model including road, driver and manoeuvres.

All the parameters for the vehicle model subsystems (i.e., engine, drivetrain, brakes, suspension, tires, etc.) are parameterized by a parameter set. For the Demo 4 simulations, the "MidSizeCar" sample parameter set (already provided by default in dSPACE's ModelDesk and available in Figure 33) is used as a basis. The most relevant parameters for the concerned simulations are modified in order to represent the real vehicle used in the physical tests (i.e., Toyota RAV4). These parameters include:

- Geometry, mass and inertia parameters.
- Tyre parameters based on the Pacejka's Magic Formula (Pacejka, 2012).
- Brake system parameters.
- Driver parameters, specifically related to lateral control.



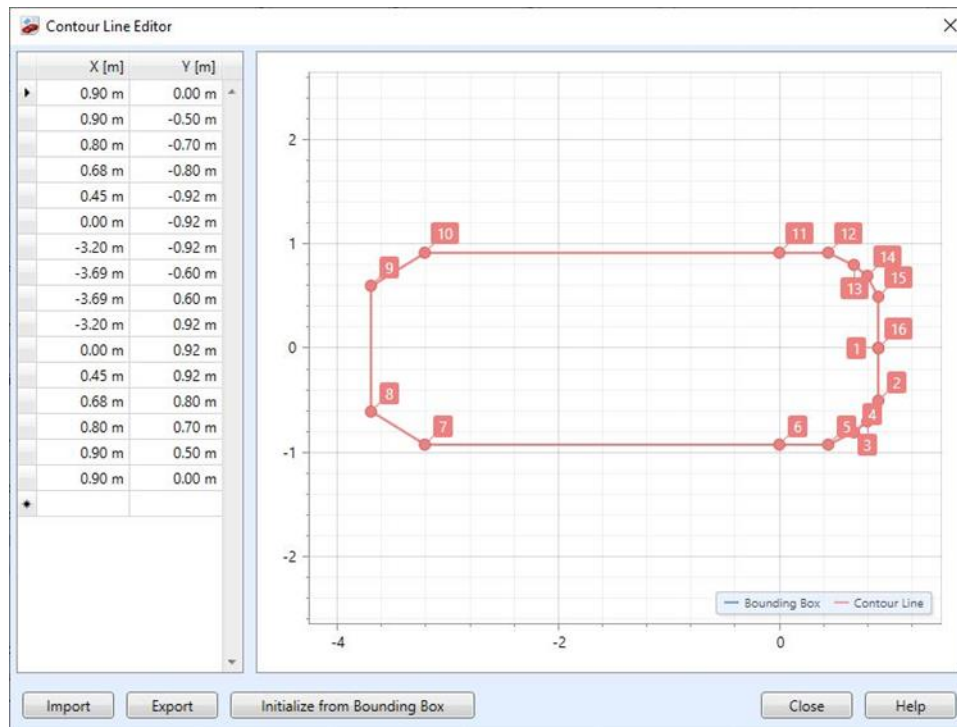


Figure 35: Vehicle geometry contour. The vehicle front is on the right side of the Figure.

To simulate additional traffic participants such as VRUs, traffic vehicles or traffic objects (i.e., obstructions), as well as vehicle sensors, dSPACE's ASM Traffic model has been used.

ASM Traffic provides a library with EuroNCAP objects. Among the objects provided in this library, the adult pedestrian (EPTa) and the bicycle (EBT) have been used. These objects are already compliant with the geometries defined in the EuroNCAP protocol TEST PROTOCOL – AEB/LSS VRU systems Version 4.2 (Euro NCAP, 2022b), see Figure 28 in Section 4.1.2.2.

5.1.3.3 Sensor and Perception model

Two kinds of Sensor and Perception models are used by ZF for the performance assessment.

The baseline model represents a SOTA sensor camera only perception system. This model has been chosen, since the implemented real sensor-set with its perception is under disclosure. The sensor itself can be modelled with a FOV definition, see Figure 36. A CarMaker internal pixel-based perception is used. This model provides the confidence and the type of detected objects.

The treatment sensor model with RSU-System is idealized by ground truth sensor. All objects in the near field of the vehicle are known and available for the function.

As stated in the section above, IDIADA is using dSPACE's ASM Traffic tool which provides the capability to simulate vehicle sensors. For the simulations in Demo 4 the "Object 3D



Sensor” provided is parametrized to match the FOV (field of view) of the sensors fitted to the real vehicle (see Figure 36).

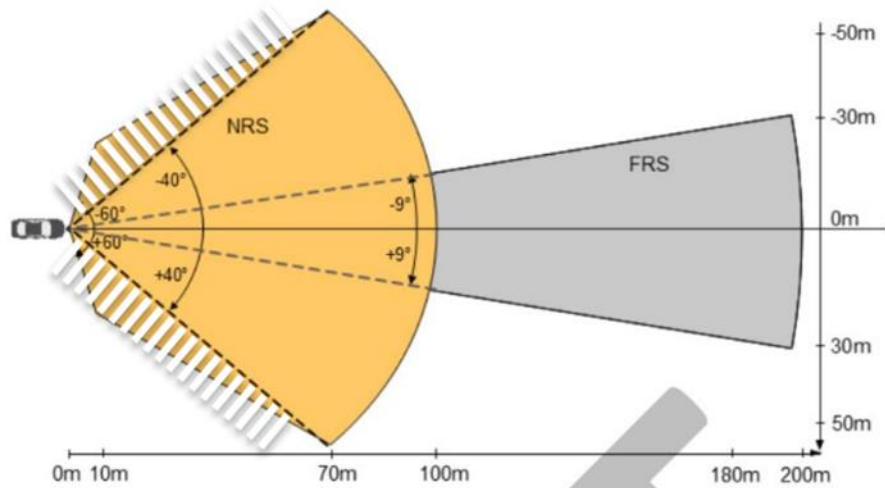


Figure 36: Field of View of Near Range Sensor (NRS) and the Far Range Sensor (FRS) the sensors fitted in the real vehicle.

Parametrization is made to obtain an ideal behaviour of the sensor, meaning that any object found within the FOV of the sensor will be detected and classified, without any error or uncertainty regarding its existence, classification or ground truth position, as represented in Figure 37.

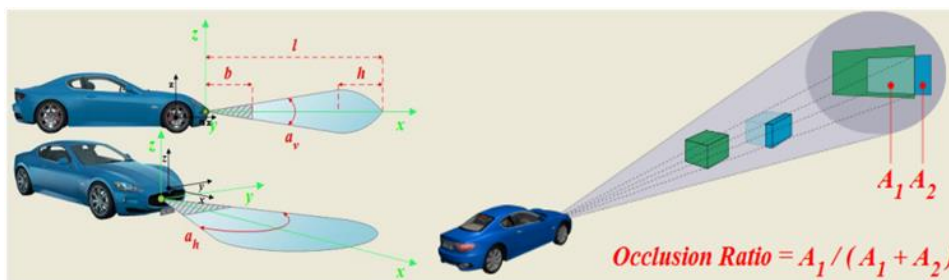


Figure 37: Representation of some of the parameters of the Object 3D sensor utilized in the simulations.

5.2 Physical testing

5.2.1 Real VRUs (cyclists) using an enhanced VRU V2X device and a virtual vehicle

In this setup, real cyclists ride a bike which has a VRU device integrated. Such device uses its own sensors and also the bike’s sensors to perform calculations of collision-risk situations



in order to provide an on-time warning to the user. The scene contains a virtual vehicle which sends V2X information to the VRU device to let it know where it is and simulate a collision trajectory with the VRU in all scenarios.

For this setup, all Demo 4 scenarios (Section 5.1.1) are executed with a reduced set of speeds for both the (virtual) vehicle and the VRU. More information about this test can be found in D3.7 (Nikolaou et al., 2021). The resulting reaction times and times to stop of this analysis shall be used in the simulations to answer Demo 4 RQ1.

5.2.2 Dummy VRU platforms and real vehicle

The physical testing of Demo 4 was performed by IDIADA and is described in detail in D3.7 (Nikolaou et al., 2022). In this section the tests performed with the dummy VRU platforms and real vehicle are described. In these tests no real users are involved. Pedestrian and cyclist testing dummies are synchronized with a real vehicle (VuT) in order to make them have colliding trajectories, as it is done for EuroNCAP tests, following all Demo 4 scenarios' parameters. This setup has three testing configurations:

- **Baseline:** The VuT and VRU are not equipped with V2X technology. The purpose of this test is to evaluate the performance of the AEB system of the VuT for the Demo 4 scenarios.
- **Connected VRUs:** The pedestrian and cyclist dummy platforms are equipped with a VRU V2X device and the VuT is equipped with V2X technology as well. In these tests, a direct communication between the VRU and VuT is expected to improve the baseline performance of the AEB, especially in those runs at higher speeds. All Demo 4 scenarios include obstructed or low visible VRUs, which are the scenarios most suitable to assess the benefit of a V2X technology in safety-critical situations. The dummies platforms will carry a VRU device.
- **Non-connected VRUs:** The scenario is monitored from a RSU with perception capabilities. This RSU will inform the VuT via V2X technology about the presence of the VRUs (pedestrian and cyclist dummies), which won't have V2X capabilities. This indirect communication will allow to assess whether road-side technology can have enough performance to replace VRU V2X devices carried by the users.

During the preparation for these tests, the test matrix for each scenario was created. The detailed parameters and the status of the devices/connectivity for every run is available in Appendix A of D3.7 (Nikolaou et al., 2022). The main objective was having a baseline (no V2X), a direct VRU connectivity and an indirect connectivity (via RSU) for each of the runs from Demo 4 scenarios.



6. Common aspects

In this section the common aspects of the assessment method that are not specific to a single Demo, i.e., are relevant for multiple demonstrators are described. This includes combination of test results and simulation results for a specific Demo, aspects of extrapolation method and aspects of market penetration.

6.1 Bayesian modelling

A key aspect in this project is to combine results from different sources concerning the effectiveness of the SAFE-UP systems in different scenarios, i.e., simulation results and test results. This includes combination of simulation results and test results for a specific Demo, which are relevant for Demos 3 and 4 separately. Bayesian statistical methods have been identified as an appropriate mathematical framework for this purpose as they provide a mathematically optimal way of updating prior information with new observations, as long as the mathematical representations of the prior information and the sampling model represent a rational person's beliefs (Hoff, 2009). In the next paragraph, the Bayesian statistical approach is described briefly on a conceptual level, based on Equation (9) below. This equation is included primarily in order to introduce the terminology used in Bayesian inference and it is not essential to understand the mathematical details of equation (9) in order to follow the assessment method.

Bayesian models are based on the following equation called Bayes' rule:

$$p(\theta|y) = \frac{p(y|\theta)p(\theta)}{\int_{\theta} p(y|\tilde{\theta})p(\tilde{\theta}) d\tilde{\theta}} \quad (9)$$

In this setting, θ is a numerical parameter that needs to be estimated. In the right-hand side of the equation, $p(\theta)$, called the *prior distribution*, is a probability distribution representing prior information regarding the probability of different values of θ (which could potentially originate from expert opinion, previous experiments, or from other information sources). Further, $p(y|\theta)$ represents the sampling model describing the probability of a new outcome y given a fixed value of θ being the true parameter. The integral in the denominator is constant in θ , where $\tilde{\theta}$ is merely a reminder that the denominator's is distinct from the specific θ value in the numerator (Hoff, 2009). These quantities determine the *posterior distribution* $p(\theta|y)$ which represents our updated beliefs about the probability of different values of θ after having observed the new outcome y . Further details about Bayesian methods can be found e.g., in (Kruschke, 2015) or in (Hoff, 2009) whose terminology is used throughout this report. To summarize, Equation (9) is the mathematical formulation of how prior beliefs about an unknown parameter θ , represented by the prior distribution $p(\theta)$, are updated based on new information y , yielding the posterior distribution $p(\theta|y)$. In the benefit assessment method in SAFE-UP, simulation results, described in Section 4.1 and 5.1, will be considered as prior information about the SAFE-UP systems and this will be updated



with test results as new observations (see Section 6.1.3). As the characteristics of the use cases can be generally different, modelling occurs on use case level per Demo, i.e., separately for Demo 3 and separately for Demo 4.

For each use case, two models are considered: one estimates the probability of the collision avoidance by the safety system and the other model estimates the collision speed, given that the collision is not avoided. Simulation results provide sufficient information to construct priors for these models, and the general idea was to update these priors based on the test results. Sections 6.1.1 and 6.1.2 contain detailed descriptions of the aforementioned models.

6.1.1 Modelling the probability of crash avoidance

For each use case and algorithm, a model is developed based on the simulation results to estimate the probability of crash avoidance. This probability is updated based on the test results corresponding to the use case. The current section gives a description of building the model and the update process and the mapping between use cases and tests is specified in Section 6.1.2 below.

For a fixed use case and algorithm, in the terminology of the previous section, the probability of avoiding a crash is modelled as a logistic regression dependent on available predictors, e.g., those listed in Section 6.1.2 below. However, in order to have a match between simulation and test cases, the dependence on the predictors such as initial speed of the car (initial speed of the VRU, and lateral position) is taken into account for this model. The logistic regression fits a coefficient for each predictor and an overall intercept as in the equation below, where β_i represents the coefficient for predictor x_i ($i = 1, \dots, k$ is the index representing the i -th predictor):

$$p = \frac{1}{1 + e^{-(\beta_0 + \beta_1 x_1 + \dots + \beta_k x_k)}} \quad (10)$$

In order to fit Equation (10), various initial speeds are considered that correspond to the initial speeds used in the demonstrator tests and in such a way that for each considered initial speed, there is a sufficient number of cases.

The posterior distribution can then be specified for each fixed use case, algorithm and initial speed value which allows the identification of estimates and confidence intervals for the parameters. The posterior, in turn, will be used as the prior in models of the physical tests. For that model, the variances on the priors will be increased so that the sample size of the simulations does not overwhelm the estimation using the physical tests. The assumption is that physical tests are more realistic and thus should be given higher weight (via relaxing the priors that came from the simulations).

6.1.2 Modelling collision speed in case of a crash

For each use case and each algorithm, a linear regression model (or other standard regression model) can be built to model the collision speed when the crash is not avoided.



The motivation for constructing such a model as opposed to using the observed collision speeds in simulations is threefold: 1) the regression model yields confidence intervals and can be used to consider best-case and worst-case scenarios; 2) the model can be applied to those crashes which were avoided in the simulations but based on the probabilistic model proposed in Section 6.1.1 may have a nonzero probability of ending up in a crash; 3) the linear regression model is well suited to a Bayesian update with new information.

A larger set of variables can be considered as covariates when constructing the model, as follows:

- Initial speed of the car;
- Initial speed of the VRU;
- Longitudinal distance;
- Lateral distance.

All subsets of these variables can be considered as covariates and the linear regression model with the lowest Akaike Information Criterion (AIC) value (Akaike, 1974) can be selected as a final model.

6.1.3 Test results chosen

The goal of the vehicle-based testing activities on closed test tracks is to evaluate the performance of the developed prototypes in the addressed scenarios.

The prototypes are equipped with sensor and actuator technologies and algorithms that go beyond what is available on the market today and are detailed in D3.6 (Löffler, Gloger, et al., 2022) and D3.7 (Nikolaou et al., 2022).

The developed test protocol is aligned with current consumer testing procedures. This requires all tests to be conducted with driving robots, including a steering robot as well as brake and acceleration actuation. This allows the vehicle dynamics to be controlled over the whole test run within tight accuracies and ensures high repeatability of each run.

The scheduled test cases are described in Section 4.2 and 5.2. The features implemented in the developed systems are described more in detail in D3.6 (Löffler, Gloger, et al., 2022) and D3.7 (Nikolaou et al., 2022).

The general idea of updating simulation results with test results in a Bayesian framework requires matching of test scenarios to the use cases. The matching used in the assessment method is specified in Table 16 below.



Table 16: Matching of test scenarios and use cases.

Test scenario	Represented use case	VRU type
Demo 3	PRwoSO	Pedestrian
Demo 3, Demo 4	PRwSO	Pedestrian
Demo 3	PLwoSO	Pedestrian
Demo 3, Demo 4	PLwSO	Pedestrian
Demo 3	CRwoSO	Cyclist
Demo 3, Demo 4	CRwSO	Cyclist
Demo 3	CLwoSO	Cyclist
Demo 3, Demo 4	CLwSO	Cyclist

The simulation results for a use case are updated with the test results for the matched test scenarios as described in Section 6.1. The updated results are used to estimate the crash frequency at different collision speeds for cars equipped with the SAFE-UP systems. This is combined with the risk of injuries of various severities at given collision speed values, which are specified by injury risk functions, as described in Sections 1.1.4.1 and 1.1.4.2 for pedestrians and cyclist, respectively.

6.1.4 Injury risk functions

As indicated in the introduction (Section 1.1), literature review of injury risk functions (IRF) were performed and the IRFs for cyclist and pedestrians selected in Section 1.1.4 are used in the estimation of the benefit.

6.1.5 Estimation of the posterior benefit

The computation of the safety benefit of the SAFE-UP systems is based on the combination of the models described in Section 6.1 with the injury risk curves specified in the Section 1.1.4, using a variant of the dose-response model (Bálint et al., 2013; Korner, 1989; Kullgren, 2008). This model estimates the number of people with injuries of a given type or severity based on crash frequency and injury risk, with respect to a crash severity parameter which in this report is selected to be the collision speed.

The dose-response model estimates the number of VRUs sustaining an injury of the given severity within the use case, denoted by $E(N)$, as follows:

$$E(N) = \int_0^L f(v)r(v) dv \quad (11)$$



where v is the collision speed; $f(v)$ is the crash frequency at v (the number of car-to-VRU crashes within the use case occurring at collision speed v); $r(v)$ is the risk of sustaining an injury of the given severity, and L is the largest value v such that $f(v) > 0$ (i.e., the highest collision speed value within the use case). In this formula, the dependence of these quantities on the use case is suppressed in the notation for simplicity. $f(v) > 0$ As SAFE-UP systems can potentially avoid a crash or change the collision speeds for those crashes that cannot be avoided, for their assessment, $f(v)$ needs to be replaced by a new crash frequency function $f_{new}(v)$; the details of how to compute this function are described below, see Equation (12). Assuming, that this function is known, an estimate corresponding to $E(N)$ can be computed using the same injury risk function $r(v)$ but replacing the original crash frequency function $f(v)$ in (11) by $f_{new}(v)$.

For the assessment method described in this report, the original crash frequency function per use case can be computed based on the collisions speeds in the crash data that was used for the simulation (see Section 4.2 and 5.1) and the injury risk functions are specified in Section 6.1.4. The way the crash frequency curve is transformed by the SAFE-UP safety systems can be estimated based on the results described in Sections 6.1.1 and 6.1.2 as follows. For each crash c in the crash simulated data, the model developed in Section 6.1.1 specifies a probability $p(c)$ of the crash being avoided, and an estimate $\tilde{v}_{coll}(c)$ regarding the collision speed in case the crash is not avoided (which happens with probability $1 - p(c)$), rounded to the closest integer value. Therefore, for a given use case denoted by UC , the transformed crash frequency function can be computed by defining, for each nonnegative integer value v , the quantity

$$f_{new}(v) = \sum (1 - p(c)) 1_{\{\tilde{v}_{coll}(c)=v\}} \quad (12)$$

where $c \in UC$ means that the crash is included in the given use case and $1_{\{\tilde{v}_{coll}(c)=v\}}$ is an indicator function taking value 1 if the estimated collision speed for the crash rounded to the closest integer equals the specified value v and 0 otherwise.

Having specified all functions as above, the dose-response model quantifies the expected number of cases with the considered injuries (e.g., fatalities, and serious injuries) per use case and per algorithm with and without the assessed system. Those can then be summarized to quantify the posterior benefit for all cyclist use cases, respectively all pedestrian use cases. Using the confidence intervals specified in the models in Sections 6.1.1 and 6.1.2 yields confidence intervals for the reductions as well.

6.2 Extrapolation

The weighting methods are applied to make the results more representative for crashes in the EU rather than the crashes in the sampling areas of the databases. For weighting the results from the GIDAS to EU level, every case in GIDAS is classified into a specific category, according to relevant variables such as: location of the crash (urban or rural), light condition (daylight or night), weather, or relation to a junction (crash happened at junction or



not at junction). Such weighting methods can be called hypercube weighting because they consider cross-tables with all combinations of the variables that could be visualized as a hypercube. All combinations of the variable values will be assigned a weighting factor corresponding to the number of crashes in CARE with the given combination of characteristics, divided by the number of corresponding crashes in GIDAS. Data from CARE with the combination of characteristics can be extracted, for example, for car-to-pedestrian accidents in EU-28 in a specific year (e.g., 2018). To get analysis results that are meant to represent EU traffic, each analysed crash in GIDAS with specific values for these variables will be counted with a multiplication term specified by the weighing factor.

The hypercube weighting method was exemplified in a case-study in D 5.2 (Bálint, Schindler, et al., 2021). In the following section, a sensitivity analysis is performed exploring the sensitivity of the results to the specification of the variable selection for hypercube weighting.

6.3 Sensitivity analysis

In this section, we illustrate how the results may change if the number of variables considered in the hypercube weighting is varied, or when some variables are replaced by others. Specifically, these variables' effect on the overall reduction of future crashes compared to the original set when weighted to EU data (D2.6 (Bálint, Labenski, et al., 2021) and D5.2 (Bálint, Schindler, et al., 2021)) is analysed.

The above question is addressed in the sensitivity analysis conducted in T5.3, exploring the sensitivity of results to the specification of the variable selection for hypercube weighting. Which variable combinations can be considered are mainly determined by limitations in data availability in the in-depth data (too few cases for unusual variable combinations) and data quality in the regional data (unreliable variable values or too many unknowns for detailed variables such as crash type), as described in several reports (D5.2 (Bálint, Schindler, et al., 2021), PROSPECT D2.3 (Kovaceva et al., 2018) and OSCCAR D1.1 (Dobberstein et al., 2018)).

As mentioned, in D5.2, an analysis was performed to show how the future crash configuration would change using IGLAD (Initiative for Global Harmonization of In-depth Data project, called the IGLAD database, contains in-depth crash data from more than 10 countries worldwide, including several EU countries (IGLAD, n.d.)). Specifically, it was investigated how the current distribution of crash types may change as a result from widespread usage of active safety systems. Specifically, on the IGLAD database we manually applied active safety systems (the methodology of the manual application is described in D2.6 Section 4.4). From IGLAD database, the crashes in European countries (namely Austria, Czech Republic, Germany, France, Italy, Sweden and Spain) are extracted and their information analysed. This data serves as a baseline, i.e., to understand the current situation. In a second step, generic active safety systems that are expected to have a widespread implementation in the coming years, are applied to this dataset to identify which crashes would be avoided by the systems. In this report, as mentioned before, we perform sensitivity analysis on alternative sets of variables for weighting.



Specifically, to get analysis results that are meant to represent EU traffic, we apply weighting factors between IGLAD and CARE for three sets of variables:

1. Variable set 1: location (urban/rural), and accident severity (fatal, serious, slight).
2. Variable set 2: location (urban/rural), light condition (darkness, daylight, twilight) and accident severity (fatal, serious, slight). In comparison to the first variable set we add one more variable, i.e., light condition.
3. Variable set 3: location (urban/rural), weather condition ('dry/clear' and 'not dry') and accident severity (fatal, serious, slight). In comparison to the second variable set, we replace one variable with another.

The analysis on each of the sets of variables is explained in the following paragraphs.

Analysis on first set of variables

The first set of variables for weighting are the location (urban/rural) and the accident severity. The resulting factors between IGLAD and CARE are shown in Table 17.

Table 17: Weighting factors between IGLAD and CARE for the first set of variables.

Location	Accident Severity		
	Fatally	Serious	Slight
Urban	26.20	158.84	332.94
Rural	21.85	165.28	437.67

After applying the weights on IGLAD data, the systems show a reduction of crashes of 34.7% on European level. Figure 38 shows the distribution within the main crash type categories for the weighted data for the first set of variables.



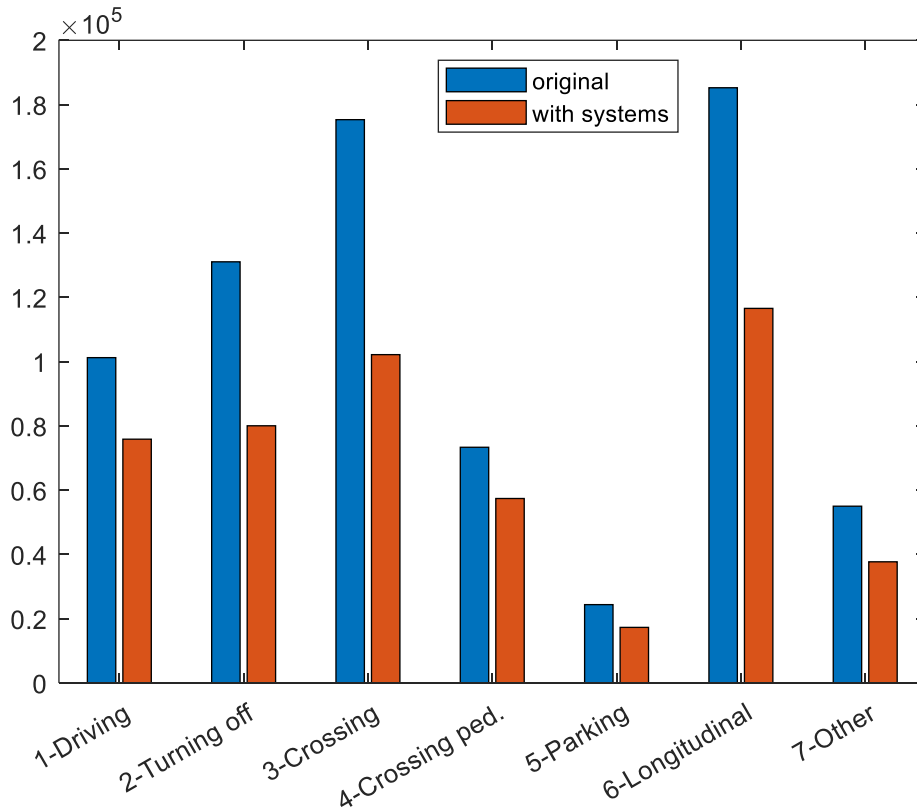


Figure 38: Crash distribution of the main crash type categorised based on weighted IGLAD data. The weights based on location, and accident severity.

Analysis on second set of variables

The same analysis is repeated now on the second set of variables: location (urban/rural), light condition (darkness, daylight and twilight) and accident severity (fatal, serious, slight).

The resulting factors between IGLAD and CARE are shown in Table 18.

Table 18: Weighting factors between IGLAD and CARE for second set of variables.

Location	Light Condition	Accident Severity		
		Fatally	Serious	Slight
Urban	Darkness	28.53	170.27	448.44
	Daylight	23.73	145.79	308.43
	Twilight	42.62	161.01	469.31
Rural	Darkness	26.91	217.13	790.37
	Daylight	20.05	135.10	400.85
	Twilight	18.54	138.10	330.43



After applying the second set of weights on IGLAD data, the systems show a reduction of crashes of 34.8% on European level. Figure 39 shows the distribution within the main crash type categories for the weighted data for the second set of variables.

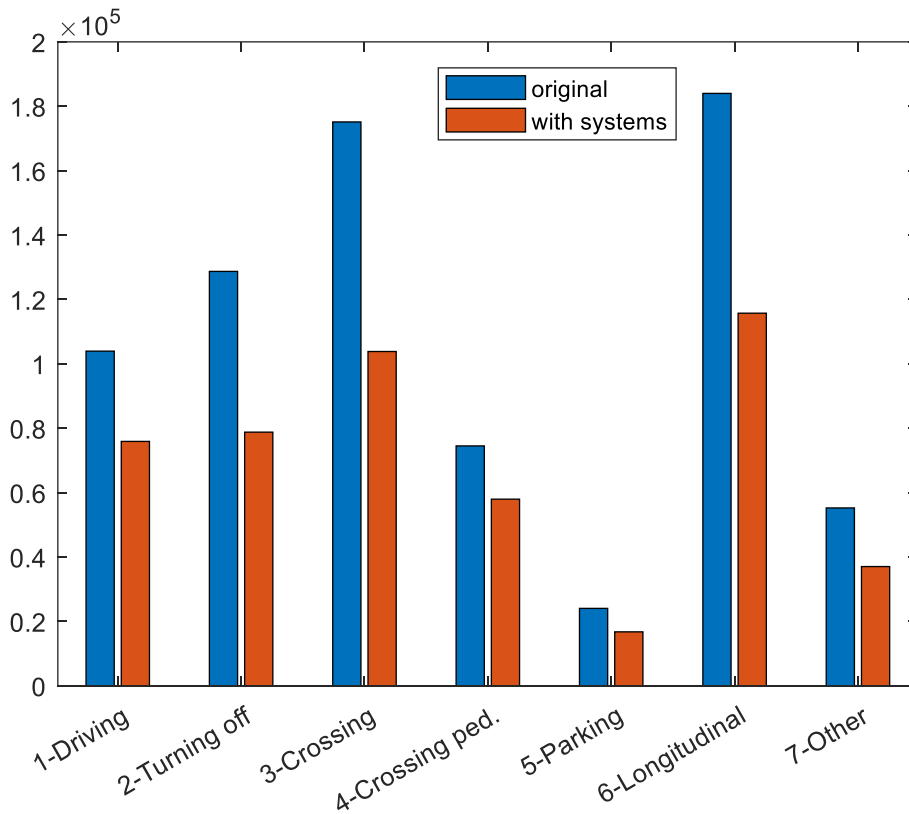


Figure 39: Crash distribution of the main crash type categorised based on weighted IGLAD data. The second set of weights based on location, light condition and accident severity.

Analysis on third set of variables

The same analysis is repeated on the third set of variables: location (urban/rural), weather condition (dry/clear and not dry) and accident severity (fatal, serious, slight).

Factors from the third set of variables are shown in Table 19.

Table 19: Weighting factors between IGLAD and CARE for third set of variables.

Location	Weather condition	Accident Severity		
		Fatally	Serious	Slight
Urban	Dry / Clear	28.47	259.66	545.90
	Not Dry	19.32	56.38	113.84
Rural	Dry / Clear	25.17	257.89	680.14
	Not Dry	14.18	63.38	191.12



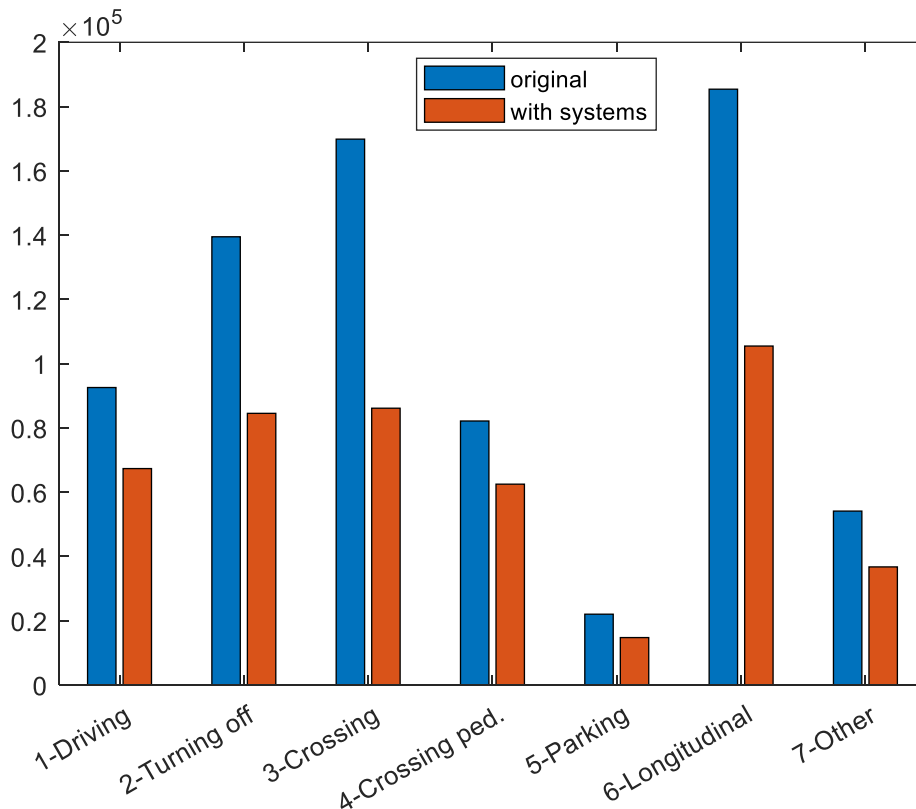


Figure 40: Crash distribution of the main crash type categorised based on weighted IGLAD data. The third set of weights based on location, weather condition and accident severity.

After applying the third set of weights on IGLAD data, the systems show a reduction of crashes of 38.6% in European level. Figure 40 shows the distribution within the main crash type categories for the weighted data for the third set of variables.

Summary

As can be seen from the above analysis, the systems will lead to a reduction of crashes on EU level of 34.7%, 34.8% and 38.6% when using weights derived from variable set 1, 2 and 3, respectively. This sensitivity analysis helps us understand the potential range of benefit of the active safety systems, which can be between 34.7% and 38.6% given all cars are equipped with the systems.

Table 20 summarizes the main crash categories for the weighted IGLAD data with the three different set of variables. It can be seen that '4-Crossing pedestrian' scenarios remain cases with the lowest percentage of avoided crashes and they increase their share in the overall crash distribution from 9.8% to 11.8% when using the variable set 1 for the weights (their share also increases when using the variable set 2 and 3 for the weights).

The percentage of crashes that are avoided by the applied active systems is largest for the '3-crossing' scenarios for the weighted data in all three variable sets. The crashes in '7-longitudinal' scenario have the highest share on the European level after applying the active



safety systems. Within the crash types, the reduction does not change much with the different set of weights.

Table 20: Overview of different crash types and the expected changes in the crash type distribution based on an analysis of weighted IGLAD data.

Variable set for the weights	Main crash type	Number of crashes in weighted IGLAD sample	% of all crashes original	% of all crashes w system	Reduction in %
Variable set 1 (location, accident severity)	1-Driving	101241	13.6	15.6	25.1
	2-Turning off	131067	17.6	16.4	38.9
	3-Crossing	175305	23.5	21.0	41.7
	4-Crossing pedestrians	73350	9.8	11.8	21.7
	5-Parking	24379	3.3	3.6	29.0
	6-Longitudinal	185234	24.8	23.9	37.1
	7-Other	55011	7.4	7.7	31.5
	Total		745587	100	100
Variable set 2 (location, light, accident severity)	1-Driving	103949	13.9	15.6	27.0
	2-Turning off	128711	17.3	16.2	38.8
	3-Crossing	175127	23.5	21.4	40.7
	4-Crossing pedestrians	74511	10.0	11.9	22.2
	5-Parking	24054	3.2	3.4	30.3
	6-Longitudinal	183989	24.7	23.8	37.1
	7-Other	55247	7.4	7.6	32.9
	Total		745587	100	100
Variable set 3 (location, weather, accident severity)	1-Driving	92563	12.4	14.7	27.2
	2-Turning off	139476	18.7	18.5	39.4
	3-Crossing	169864	22.8	18.8	49.3
	4-Crossing pedestrians	82146	11.0	13.7	23.9
	5-Parking	22024	3.0	3.2	33.0
	6-Longitudinal	185405	24.9	23.1	43.1
	7-Other	54109	7.3	8.0	32.1
	Total		745587	100	100

6.4 Market penetration

The system performance and expected results are computed as described above. These results however assume 100% fleet penetration rate of the system. In general, the fleet penetration of 100% is not reached instantly but over a rather long period. As shown in (Seidl et al., 2018) for AEB systems, it takes around 10 years to reach a market penetration of 20%



This project has received funding from the European Union's Horizon 2020 research and innovation programme under Grant Agreement 861570.

and around 15 years for a penetration of 50% (see Table 21). This means that the safety benefit of the system is not reached instantly, but increases over time as the penetration rate increases. More detailed information on this topic can be found in the article from (Sander & Lubbe, 2018).

Table 21: Examples of fleet penetration rate for AEB systems for VRUs.

Safety measure	Fleet penetration (%)		
	2016	2025	2030
AEB-Cyclist	0.15	19.54	59.48
AEB-Pedestrian	1.01	37.02	73.83

Regarding penetration rates, the following assumptions may be considered: the vehicle fleet penetration rate X% (e.g., 20%), the Road Site Unit penetration rate of 100% and VRU on board penetration rate of 100%.

In this assessment, for reasons of simplicity, it shall be assumed that a market penetration of a given percentage (x%) also results in the corresponding number of reduced casualties compared to the maximum benefit (e.g., only x% percent of casualties are “really” prevented by the system).

The safety benefit can be calculated based on the avoided injuries (system performance) in consideration of a market penetration for the respective year, using the following formula:

$$SB_{year,injury} = (n_{injury}) * mp_{year}$$

where SB refers to the safety benefit, n to the number of avoided casualties per injury severity (either fatal, severe), assuming a market penetration of 100%, and mp refers to the market penetration in the respective year.

The research questions for the demonstrator technologies prescribe the analysis of safety benefit for specific values of the market penetration parameter, based on conservative (9.6%), ambitious (27.5%) and optimistic (100%) scenarios defined in the grant agreement of SAFE-UP. Another way to approach the analysis would be to study which values of this parameter are necessary to achieve a desired/prescribed level of the overall safety benefit (e.g., a 10% reduction compared to the number of fatalities and seriously injured in e.g., 2016).



7. Discussion and conclusions

As described in previous sections, the overall safety benefit assessment method has not changed compared to the preliminary framework specified in D5.1 and updated in D5.2. However, progress has been made regarding understanding and planning of the analysis for the elements of the framework. Further work in T5.3, described in this report, show the methods and approaches on how the simulation activities and physical testing are performed and how the results will be analysed in T5.4 in order to assess the safety benefit per Demo.

Demo 1, in summary, focuses to enhance occupant protection during collisions and minimize the increased risk of injury for occupants in new seating positions, such as reclined seatbacks, by exploring an added feature (AF) restraint system. This system is being tested in Demo 1 using virtual evaluations with both female and male Human Body Models in new seating positions, with both state-of-the-art and AF restraint systems. For assessing car occupants' injury risk, injury risk functions based on injury criteria for individual body regions such as head, and rib have been selected from the literature. Furthermore, a new injury risk function for compression lumbar spine injuries has been constructed for the updated VIVA+ model in SAFE-UP in T5.2 and is used in this report. The results of the application of the method and the evaluation results are reported in D5.4.

Demo 2 focuses on the development of weather filter which is used to assess the effect of advances of increased visibility, of primarily pedestrians and bicyclists, in sensor technologies in adverse weather conditions. To achieve this, physical testing is carried out under various weather conditions, including adverse weather conditions such as rain and fog. Demo 2 itself did not develop a technology but enables the assessment of weather effects in various scenarios. The test results are used to develop a filter representing reduced sensor performance in such weather conditions which is then included in pre-crash simulations. The assessment itself concentrates on reduced FOVs in rainy and foggy situations. The FOV-models have been generated by physical static measurements.

Demo 3 focuses on the development of an Autonomous Emergency Braking and Steering system (AEB+S). The scenarios addressed by Demo 3 are selected based on the theoretical possibility of avoiding crashes by braking and steering under given boundary conditions. The safety systems for VRU protection are integrated in a co-simulation platform, which is used to obtain results for safety benefit assessment. The results are further supported by physical testing of the Demo 3 vehicle.

Demo 4 focuses on investigating the safety benefits of Cooperative Intelligent Transport Systems (C-ITS) by considering all possible communication interactions, such as warnings to both vulnerable road users and drivers, as well as activation of safety systems like AEB for VRU protection. The demonstrator includes physical testing of the Demo 4 vehicle in relevant scenarios and virtual performance assessment of the benefits of V2X as an additional sensor node for the vehicle system. Demo 4 simulation assessment is not involving the signal flow and the lack for the C-ITS System and does not involve the



synchronous GNSS positioning of the V2X VRU device. The simulations' assessment of ZF and IDIADA are considering an idealized V2X-System.

In addition to the specific assessments for each Demo, the report also covers elements of the assessment that are not tied to any single Demo. For example, the report covers the combination of test results and simulation results, as well as methods for extrapolating results from locally collected data to the EU level and considering market penetration. The report also includes a sensitivity analysis that examines how the results are affected by the specifications used in the weighting method, such as the selection of variables for hypercube weighting. Additionally, the report describes the use of the statistical approach from the PROSPECT project, which combines test results and simulation results using a Bayesian statistical approach.

In D5.1 it has been motivated that the method developed in the PROSPECT project based on Bayesian statistical methods is appropriate for this purpose. Further, this method has suitable interfaces required by the initiative P.E.A.R.S. for harmonization of active safety systems assessment, (Page et al., 2015). This report D5.8, further specifies the details of the underlying mathematical models that will be used in the method for SAFE-UP systems (see Section 6.1). The advantage of using virtual simulations is that they are risk-free, reproducible, time-efficient and allow performing multiple tests. At the same time, the quality of results depends on how well the implemented models represent reality. On the other hand, the prototype real-world testing includes real vehicles and environment but a limited number of tests. The relatively low number of tests makes it challenging to understand the transformation of the crash frequency for the full range of crash severity values. Combining the results from both virtual simulations and real-world testing as described in this deliverable allows the utilization of the advantages of each data type. It also helps overcoming some of the challenges inherent in methods based on a singular data type. Using knowledge synthesis from simulations and tests, it is possible to derive more comprehensive and representative conclusions regarding safety benefit of the SAFE-UP systems.

In conclusion, the next step is to apply the methodology outlined in this report on the simulations and physical tests performed in T5.4 and report the safety benefit of the SAFE-UP Demos in D5.6.



Bibliography

- Akaike, H. (1974). A New Look at the Statistical Model Identification. *IEEE Transactions on Automatic Control*, 19(6), 716–723. <https://doi.org/10.1109/TAC.1974.1100705>
- Althoff, M., & Würsching, G. (2020). *CommonRoad: Vehicle Models*.
- Bálint, A., Fagerlind, H., & Kullgren, A. (2013). A test-based method for the assessment of pre-crash warning and braking systems. *Accident Analysis and Prevention*, 59, 192–199. <https://doi.org/10.1016/j.aap.2013.05.021>
- Bálint, A., Labenski, V., Köbe, M., Vogl, C., Stoll, J., Schories, L., Amann, L., Sudhakaran, B. G., Leyva, H. P., Pallacci, T., Östling, M., Schmidt, D., & Schindler, R. (2021). *D2.6 USE CASE DEFINITIONS AND INITIAL SAFETY-CRITICAL SCENARIOS*.
- Bálint, A., Schindler, R., Löffler, C., Wimmer, P., Kirschbichler, S., Kolk, H., Klein, C., Schories, L., Hay, J., Birkner, C., da Silva, L. J., Zimmer, A., Mensa, G., Parera, N., Rokova, S., Castells, J., Mallada, L. J., Nikolaou, S., Vogl, C., & Stoll, J. (2021). *SAFE-UP D5.2: Safety impact assessment – intermediate report*.
- Becker, J., Östling, M., Lozano, P., Klein, C., Weihmayr, D., & Wimmer, P. (2022). *Occupant Monitoring Based Restraint Strategies for Future Seating Configurations-Deliverable 4.4*.
- Cavanaugh, J. M., Zhu, Y., Huang, Y., & King, A. I. (1993, November). Injury and Response of the Thorax in Side Impact Cadaveric Tests. *SAE Technical Paper Series*. <https://doi.org/10.4271/933127>
- Chajmowicz, H., Saadé, J., & Cuny, S. (2019). Prospective assessment of the effectiveness of autonomous emergency braking in car-to-cyclist accidents in France. *Traffic Injury Prevention*, 20(sup2), S20–S25. <https://doi.org/10.1080/15389588.2019.1679797>
- Craig, M., Parent, D., Lee, E., Rudd, R., & Takhounts, E. (2020). Injury Criteria for the THOR 50 th Male ATD. In *Nhtsa* (Issue September).
- Cuny, S., Chajmowicz, H., Yong, K., Hermitte, T., Lecuyer, E., & Bertholon, N. (2018). A Tool to Assess Pedestrian Safety: Risk Curves by Injury Severity and their Confidence Intervals for Car-to-Pedestrian Front Collision. *Proceedings of the International IRCOBI Conference on the Biomechanics of Impact*.
- Dobberstein, J., Lich, T., & Schmidt, D. (2018). *Accident data analysis - remaining accidents and crash configurations of automated vehicles in mixed traffic*. 768947.
- EC. (2019). *Community database on Accidents on the Roads in Europe*.
- Eppinger, R. H. (1989, October). On the Development of a Deformation Measurement System and Its Application Toward Developing Mechanically Based injury Indices. *SAE Technical Paper Series*. <https://doi.org/10.4271/892426>
- Eppinger, R. H., Marcus, J. H., & Morgan, R. M. (1984, April). Development of Dummy and Injury index for NHTSA's Thoracic Side Impact Protection Research Program. *SAE Technical Paper Series*. <https://doi.org/10.4271/840885>
- Eppinger, R., Sun, E., Bandak, F., Haffner, M., Khaewpong, N., & Maltese, M. (1999). *Development of Improved Injury Criteria for the Assessment of Advanced Automotive Restraint Systems*.



- Euro NCAP. (2022a). *Assessment Protocol - Safety Assist Collision Avoidance* (Issue July 2022). <https://cdn.euroncap.com/media/70314/euro-ncap-assessment-protocol-sa-collision-avoidance-v101.pdf>
- Euro NCAP. (2022b). *TEST PROTOCOL – AEB/LSS VRU systems, Implementation 2023* (Issue Version 4.3).
- EURO NCAP. (2021). *EUROPEAN NEW CAR ASSESSMENT PROGRAMME (Euro NCAP) - TEST PROTOCOL – AEB Car-to-Car systems* (Issue November 2022). <https://cdn.euroncap.com/media/62794/euro-ncap-aeb-c2c-test-protocol-v303.pdf>
- Forman, J. L., Kent, R. W., Mroz, K., Pipkorn, B., Bostrom, O., & Segui-Gomez, M. (2012). Predicting rib fracture risk with whole-body finite element models: Development and preliminary evaluation of a probabilistic analytical framework. *Annals of Advances in Automotive Medicine*, 56, 109–124.
- Hoff, P. D. (2009). *A First Course in Bayesian Statistical Methods*. Springer New York. <https://doi.org/10.1007/978-0-387-92407-6>
- Hussain, Q., Feng, H., Grzebieta, R., Brijs, T., & Olivier, J. (2019). The relationship between impact speed and the probability of pedestrian fatality during a vehicle-pedestrian crash: A systematic review and meta-analysis. *Accident Analysis and Prevention*, 129, 241–249. <https://doi.org/10.1016/j.aap.2019.05.033>
- IGLAD. (n.d.). *Information about the Initiative for the Global Harmonisation of Accident Data*. Retrieved October 26, 2019, from <http://www.iglad.net/>
- Iraeus, J., & Lindquist, M. (2015). Pulse shape analysis and data reduction of real-life frontal crashes with modern passenger cars. *International Journal of Crashworthiness*, 20(6), 535–546. <https://doi.org/10.1080/13588265.2015.1057005>
- Iraeus, J., & Lindquist, M. (2016). Development and validation of a generic finite element vehicle buck model for the analysis of driver rib fractures in real life nearside oblique frontal crashes. *Accident Analysis and Prevention*, 95, 42–56. <https://doi.org/10.1016/j.aap.2016.06.020>
- Iraeus, J., & Lindquist, M. (2021). Analysis of minimum pulse shape information needed for accurate chest injury prediction in real life frontal crashes. *International Journal of Crashworthiness*, 26(6), 684–691. <https://doi.org/10.1080/13588265.2020.1769004>
- ISO/TR 21934. (2021). *Road vehicles — Prospective safety performance assessment of pre-crash technology by virtual simulation — Part 1: State-of-the-art and general method overview*.
- Kemper, A. R., McNally, C., Kennedy, E., Manoogian, S., Rath, A., Ng, T., Stitzel, J., Smith, E., Duma, S., & F, M. (2005). Material properties of human rib cortical bone from dynamic tension coupon testing. *Stapp Car Crash J.*, 49, 199–230.
- Kemper, A. R., McNally, C., Pullins, C. A., Freeman, L. J., Duma, S. M., & Rouhana, S. W. (2007, October 29). The Biomechanics of Human Ribs: Material and Structural Properties from Dynamic Tension and Bending Tests. *Stapp Car Crash J.* <https://doi.org/10.4271/2007-22-0011>
- Korner, J. (1989). A method for evaluating occupant protection by correlating accident data with laboratory test data. *SAE Technical Papers*, 98(May), 870–884. <https://doi.org/10.4271/890747>
- Kovaceva, J., Bálint, A., Schindler, R., Schneider, A., Stoll, J., Jaussein, M., Bruyas, M.-P.,



- Puente Guillen, P., Large, D. R., Perlet, K., Petersson, M., & Esquer, A. (2018). *Assessment of the PROSPECT safety systems including socio- economic evaluation. Deliverable 2.3 in the EU project PROSPECT.* <https://ec.europa.eu/research/participants/documents/downloadPublic?documentIds=080166e5c4b5e293&appId=PPGMS>
- Kruschke, J. K. (2015). *Solutions to Exercises in Doing Bayesian Data Analysis 2nd Ed.*
- Kullgren, A. (2008). Dose-response models and EDR data for assessment of injury risk and effectiveness of safety systems. *2008 IRCOBI Conference Proceedings- International Research Council on the Biomechanics of Injury*, 3–14.
- Lau, I. V., & Viano, D. C. (1986, October). The Viscous Criterion - Bases and Applications of an Injury Severity Index for Soft Tissues. *SAE Technical Paper Series.* <https://doi.org/10.4271/861882>
- Löffler, C., & Gloger, T. (2021). *D3.2 Vehicle demonstrator for object detection in adverse weather conditions.*
- Löffler, C., Gloger, T., Smit, R., Blum, K., Stoll, J., & Vogl, C. (2022). *SAFE-UP-Deliverable 3.6 Vehicle demonstrator for trajectory planning and control for combined automatic emergency braking and steering manoeuvres including system for VRU detection, motion planning and trajectory control to enhance real world performance.*
- Löffler, C., Gloger, T., & Stoll, J. (2021). *D3.3 Vehicle demonstrator for trajectory planning and control for combined automatic emergency braking and steering manoeuvres including system for VRU detection , motion planning and trajectory control to enhance real world performance Co-Authors.*
- Löffler, C., Vogl, C., Labenski, V., & Weihmayr, D. (2022). *SAFE-UP D3.5 Vehicle demonstrator for object detection in adverse weather conditions.*
- Mayer C., Iraeus, J., Meyer, F., Mroz, K., Huang, Y., Nölle, L., Lancashire, R., & Weber, J. (2021). *OSCCAR Deliverable 3.3 - Criteria and risk functions for prediction of injury risks in new sitting positions and new crash scenarios.*
- Mensa, G., Wimmer, P., Schories, L., & Bálint, A. (2021). *D5.1 Requirements for impact assessment.*
- NHTSA. (2000). *Final Economic Assessment, FMVSS No. 208, Advanced Air Bags.*
- Niebuhr, T., Junge, M., & Achmus, S. (2013). Pedestrian injury risk functions based on contour lines of equal injury severity using real world pedestrian/passenger-car accident data. *Annals of Advances in Automotive Medicine*, 57, 145–154.
- Niebuhr, T., Junge, M., & Rosén, E. (2016). Pedestrian injury risk and the effect of age. *Accident Analysis and Prevention*, 86, 121–128. <https://doi.org/10.1016/j.aap.2015.10.026>
- Nikolaou, S., Castells, J., Mallada, J. L., Gragkopoulos, I., & Tsetsinas, I. (2022). *D3.7 Demo 4 (system for on-time warning provisions to VRUs and drivers in critical conditions).*
- Nikolaou, S., Idiada, J. C., Lorente, J., Tme, M., & Gragkopoulos, I. (2021). *D3.4 Demo 4 (system for on-time warning provisions to VRUs and drivers in critical conditions).*
- Nikolaou, S., & Panou, M. (2021). *D3.1 ACTIVE SAFETY SYSTEMS SPECIFICATION AND RISK Analysis.*
- Odriozola, M., Vilchez, S., Östling, M., D Addetta, A. G., & Merdivan, D. (2021). *SAFE-UP*



D4.1: Use Case Definition.

Pacejka, H. B. (2012). *Tire and Vehicle Dynamics*. Elsevier Science & Technology.

Page, Y., Fahrenkrog, F., Fiorentino, A., Gwehenberger, J., Helmer, T., Lindman, M., Op den Camp, O., van Rooij, L., Puch, S., Fränzle, M., Sander, U., & Wimmer, P. (2015). A Comprehensive and Harmonized Method for Assessing the Effectiveness of Advanced Driver Assistance Systems by Virtual Simulation: The P.E.A.R.S. Initiative. *The 24th International Technical Conference on the Enhanced Safety of Vehicles (ESV)*, 1–12. <http://www-esv.nhtsa.dot.gov/Proceedings/24/isv7/main.htm>

Prasad, P., & Mertz, H. J. (1985, June). The Position of the United States Delegation to the ISO Working Group 6 on the Use of HIC in the Automotive Environment. *Technical Paper Series*. <https://doi.org/10.4271/851246>

Rajamani, R. (2012). *Vehicle Dynamics and Control*. Springer {US}. <https://doi.org/10.1007/978-1-4614-1433-9>

Richardson, R., Jayathirtha, M., Donlon, J. P., Forman, J. L., Gepner, B., Ostling, M., Mroz, K., Pipkorn, B., & Kerrigan, J. R. (2020). Pelvis Kinematics and Injuries of Reclined Occupants in Frontal Impacts. *IRCOBI Conference 2020*, 499–515.

Rosén, E. (2013). Autonomous Emergency Braking for Vulnerable Road Users. *Proceedings of the International IRCOBI Conference on the Biomechanics of Impact*.

Rosén, E., & Sander, U. (2009). Pedestrian fatality risk as a function of car impact speed. *Accident Analysis and Prevention*, 41(3), 536–542. <https://doi.org/10.1016/j.aap.2009.02.002>

Saadé, J., Cuny, S., Labrousse, M., Song, E., Chauvel, C., & Chrétien, P. (2020). Pedestrian Injuries and Vehicles-related Risk Factors in Car-to-pedestrian Frontal Collisions. *Proceedings of the International IRCOBI Conference on the Biomechanics of Impact*.

Sander, U., & Lubbe, N. (2018). The potential of clustering methods to define intersection test scenarios: Assessing real-life performance of AEB. *Accident Analysis and Prevention*, 113(November 2017), 1–11. <https://doi.org/10.1016/j.aap.2018.01.010>

Seidl, M., Khatry, R., Carroll, J., Hynd, D., Wallbank, C., & Kent, J. (2018). *Cost-effectiveness analysis of Policy Options for the mandatory implementation of different sets of vehicle safety measures – Review of the General Safety and Pedestrian Safety Regulations (Technical Annex to GSR2 report SI2.733025. Final Report.)*.

Spitzhuettl, F., & Liers, H. (2016). *Methods for the creation of injury risk functions based on real world accident data*.

Takhounts, E., Craig, M., Moorhouse, K., & Hasija, V. (2013). Development of Brain Injury Criteria (Bric). *Stapp Car Crash Journal*. <https://doi.org/10.4271/2013-22-0010>

Takhounts, E., Hasijy, V., Ridella, S., Rowson, S., & Duma, S. (2011). Kinematic Rotational Brain Injury Criterion (BRIC). *22nd International Technical Conference on the Enhanced Safety of Vehicles (ESV)*.

Thompson, A. (2008). *Adaptive vehicle structures for secondary safety*.

Viano, D. C. (1989, October). Biomechanical Responses and Injuries in Blunt Lateral Impact. *SAE Technical Paper Series*. <https://doi.org/10.4271/892432>

Viano, D. C., & Lau, I. V. (1985). Thoracic Impact: A Viscous Tolerance Criterion. *SAE Technical Paper Series*.



Viano, D. C., & Lau, I. V. (1988). A viscous tolerance criterion for soft tissue injury assessment. *Journal of Biomechanics*, 21(5), 387–399. [https://doi.org/10.1016/0021-9290\(88\)90145-5](https://doi.org/10.1016/0021-9290(88)90145-5)

Volvo Cars. (2022). *XC40 Owner's manual* (Vol. 1, Issue March).

Willinger, R., Deck, C., Meyer, F., Wei, W., Serre, T., Aranda, R., & Peldschus, S. (2020). *Report on injury risk assessment procedures* (Issue D 2.2).

